Analytica Chimica Acta 1042 (2018) 93–108

Contents lists available at ScienceDirect

Analytica Chimica Acta

journal homepage: www.elsevier.com/locate/aca

Sensitive and selective non-enzymatic detection of glucose by monodispersed NiO @ S-doped hollow carbon sphere hybrid nanostructures

Rajesh Madhuvilakku, Ramalakshmi Mariappan, Srinivasan Alagar, Shakkthivel Piraman*

Sustainable Energy and Smart Materials Research Lab, Department of Nanoscience and Technology, Science Campus, Alagappa University, Karaikudi, 630 003, Tamil Nadu, India

HIGHLIGHTS

- The NiO@SDHCNSs hybrid nanocomposites were prepared by simple hydrothermal method.
- The obtained nanocomposites were employed to develop non-enzymatic glucose sensor.
- The resulted sensor exhibited good selectivity and reproducibility.
- A wide linear range (0.001−13 mM) with low detection limits (~52 nM) was demonstrated.
- The practical determination of glucose in blood serum and urine samples were also demonstrated.

GRAPHICAL ABSTRACT

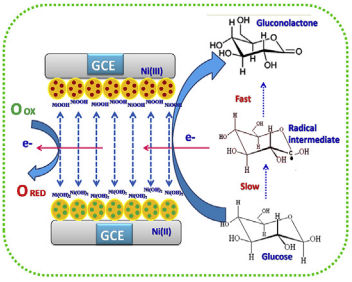

ARTICLE INFO

Article history:
Received 17 January 2018
Received in revised form
8 August 2018
Accepted 15 August 2018
Available online 20 August 2018

Keywords:
Non-enzymatic sensor
Glucose
Blood samples
Amperometry
NiO@SDHCNSs
Hollow spheres

ABSTRACT

Development of selective, sensitive and non-enzymatic sensor for glucose determination is highly important for the diagnosis and management of diabetes. Herein, we have reported the novel ultra sensitive and non-enzymatic sensor development by in-situ wraped NiO nanostructures (~10−15 nm) on the sulfur-doped hollow carbon nanospheres (SDHCNSs) through hydrothermal-assisted process. The structural and morphological properties of the nanocomposites were characterized by X-ray diffraction (XRD), Raman spectroscopy, field emission scanning electron microscopy (FE-SEM), transmission electron microscopy (TEM) and X-ray photoelectron spectroscopy (XPS) techniques. The prepared NiO@SDHCNSs was directly used as an electrochemical sensor for glucose determination, and its performance was evaluated by cyclic voltammetry and amperometric techniques. The fabricated non-enzymatic biosensor was exhibited remarkably good sensitivity (1697 μA $mM^{-1}cm^{-2}$), low detection limit (LOD) (52 nM), a wide linear range (up to 13 mM) of glucose with desirable selectivity, stability and reproducibility. Further, the constructed sensor has demonstrated an excellent anti-interference property in the presence of common interferences such as dopamine (DA), uric acid (UA) and ascorbic acid (AA). Most interestingly, the fabricated electrode is applicable for the practical analysis of glucose in the real blood serum and urine samples. The excellent electrochemical performances of NiO@SDHCNSs towards the oxidation of glucose are attributed to the increased electron transfer passage through unique hollow spherical morphology with increased redox couple of $Ni(OH)_2$/NiOOH derived from NiO. Thus, the

* Corresponding author.
E-mail address: apsakthivel@yahoo.com (S. Piraman).

https://doi.org/10.1016/j.aca.2018.08.032

improved electrochemical performances of NiO@SDHCNSs can be adopted as a potential electrode for the real sample analysis.

1. Introduction

It is well-known that the insulin is a peptide hormone which controls the glucose level in the bloodstream. When the insulin secretions are not properly regulated, metabolic diseases such as diabetes is developed [1]. Diabetes is one of the most widespread diseases that affect the human population globally. The World Health Organization has reported that around 347 million people in the worldwide suffering from diabetes [2]. The amount of glucose level in whole blood for healthy individuals is between 3.9 and 6.1 mM, while in a diabetic patient it is more than 6.1 mM [3]. Precise monitoring of the glucose level at point-of-care lower level of blood-glucose measurement is important and necessary to manage diabetes. Longtime high level of blood glucose can lead to the eye, kidney, heart, blood vessels and nerve chronic damages. Therefore, the quantitative precise detection of blood glucose is highly significant in the clinical analysis [4] (Scheme 1).

As a result, much attention has been paid to develop sensitive, selective, and cost-effective glucose sensors for in-vitro or in-vivo glucose measurement. So far, several methods based on fluorescence [5], optical [6], acoustic [7], surface plasmon resonances [8], electronic [9] and electrochemical methods have been explored for the determination of glucose. Among such methods, electrochemical methods have been widely used due to their simplicity, selectivity, high sensitivity, quick measurement, low cost, and portability [10–12]. Majority of the conventional biosensors [13–15] for glucose monitoring is involved the use of glucose oxidase (GOD) or glucose dehydrogenase enzymes in which glucose molecules react with saturated oxygen in the blood to produce gluconolactone and hydrogen peroxide (H_2O_2) under mild conditions [16]. However, the glucose oxidase is sensitive to various environmental factors, such as temperature, humidity, and pH [17]. Moreover, the immobilization as well as degradation of glucose oxidase is a complicated and expensive process. However, these enzymatic sensors could not be reused for the continuous glucose monitoring because of the adsorption of proteins from blood and also the poor stability of the enzyme, additionally the interference of some electro-oxidizable species found in blood [18]. Because of these issues, it is highly necessary to develop a non-enzymatic glucose sensor which seems to be an alternative technique for blood glucose analysis. Especially, the synthesis of an excellent catalyst for the direct electro oxidation of glucose is the crucial step in the construction of non-enzymatic glucose sensors.

To date, various micro/nanostructured materials especially

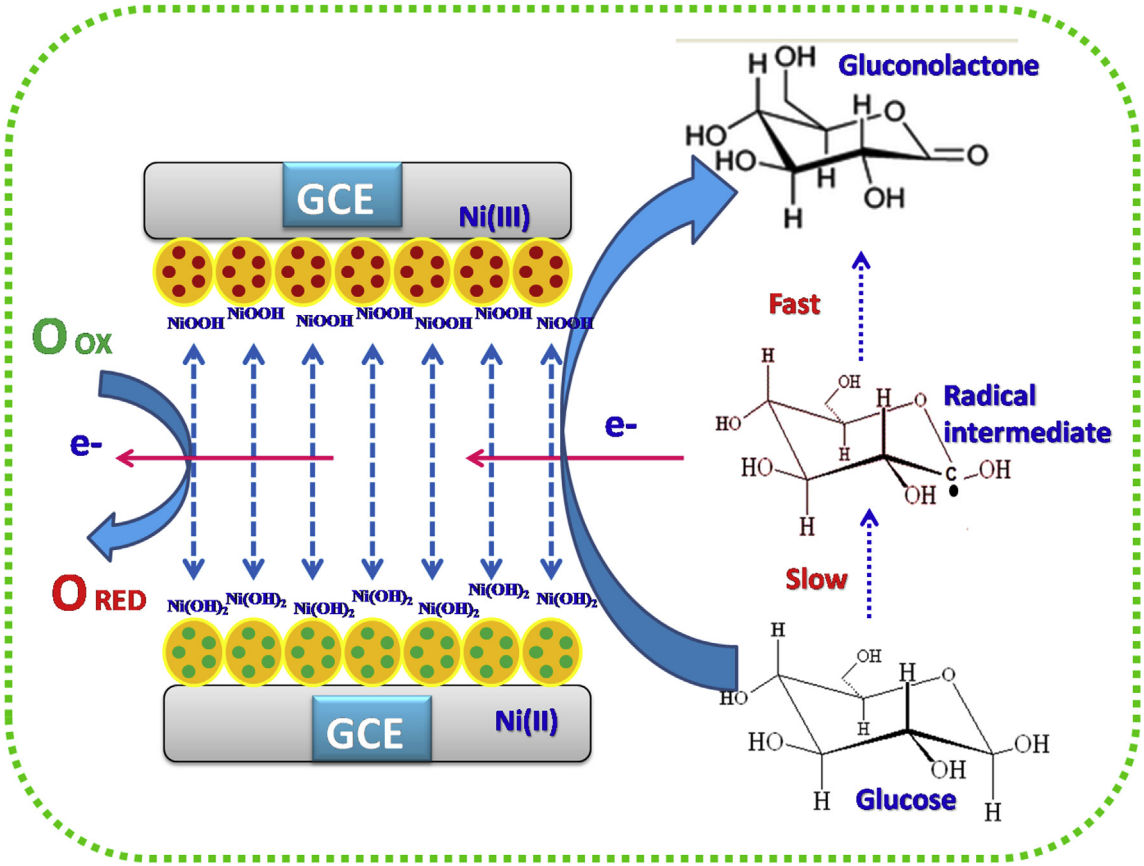

Scheme 1. Schematic diagram of a suggested mechanism for the oxidation of glucose at a NiO@SDHCNSs modified electrode in alkali.

noble metals (Pt, Au, Pd, Ru and Rh), and metal alloys (Pt-Au, Pt-Ru, Ni-Pd and Pt-Pb) have been explored as electrode materials to develop enzyme-free glucose sensor and exhibited good analytical performance for glucose detection [19]. Nevertheless, these precious metal electrodes are suffering from slow kinetics and surface fouling due to the absorption of intermediates and chloride ion leads to poor operational stability [20]. In addition, the high cost of electrode materials limiting their commercial applications, hence the ability to produce glucose sensor in large numbers at low cost is a major market requirement.

To alleviate the above-discussed problems, recently many glucose sensors were developed using various non-noble metal compounds such as Co, Ni, Cu, NiO, CoO_4, WO_3, TiO_2, Cu_2O, CeO_2, RuO_2, MnO_2 and ZnO, etc, [21]. Among these materials, enzyme-free electrochemical oxidation of glucose is greatly enhanced at Ni, NiO or $Ni(OH)_2$ based electrode due to their inherent redox behaviour (Ni^{2+}/Ni^{3+}), oxyhydroxide species (NiOOH) formation in alkaline medium, high electro-active surface area, biocompatibility and relatively low-cost, making it suitable for the fabrication of sensors in batch [22,23]. Therefore, several Ni nanoparticles based enzyme-free biosensors for glucose have been reported which showed great enhancement in the electro-oxidation of glucose compared to other metallic nanoparticles based electrodes [24,25]. Lu et al. [17], has been reported the application of nano-Ni nanowire arrays modified electrode for the amperometric sensing of glucose. Similarly, a 3D-porous nickel nanomaterial was proposed as a non-enzymatic electrochemical glucose sensor [26]. However, the gradual diminishing of Ni-based electrodes catalytic activity and surface fouling problems raised from the Ni nanostructure formed close-packed structure after assembled on the electrode surface which would reduce their specific surface area and electrocatalytic activity and thus hinders their electrochemical performances [22]. To overcome these issues, novel electrode material with good operational stability and anti-fouling performances are still highly desirable in the development of Ni-based glucose sensor.

Therefore, various carbon nanostructures such as graphene [27,28], carbon nanotubes (CNTs) [29], carbon nanofiber [7,30] fullerenes [31], carbon black (CB) [32,33], printex carbon [34,35] and carbon spherical shells (CSSs) [36] have been used extensively in biosensors. However, the high cost of the equipment and safety issues regarding the synthesis procedure of graphene, CNT and fullerenes have limited the commercial applications. Therefore, carbon nanoparticles are used as an alternative to the prestigious carbon forms such as graphene, CNTs and fullerenes. In particular, hollow carbonaceous spheres have attracted great attention due to their unique properties, such as high surface-to-volume ratio, long transport length for mass and charge transport, interior voids, low density, excellent thermal, chemical stability and surface permeability etc., [37–39]. The carbon precursor employed for the preparation of carbon nanoparticles exhibits a pivotal effect on the physical and chemical properties of the final carbonaceous materials. Recent years, glucose has been used as renewable and inexpensive carbon source for carbon nanoparticles synthesis; however, the majority of the resulting carbonaceous materials are bulk carbon without functional atoms or groups in their matrix [40]. The properties of the resulting carbonaceous nanoparticles can be tuned to the doping of heteroatoms such as nitrogen, boron, and sulfur etc. It is well known that the sulfur dopants can remarkably increase the electronic conductivity through improved electron-donor performance and increased binding active sites. Recently, Karikalan et al. [1], have reported the sulfur doped carbon nanoparticles through flame synthesis and $Ni(OH)_2$ nanoparticle decorated on the carbon nanoparticles by the co-precipitation method. Obviously, this method involves a quite complicate multiple processes. However, to the best of our knowledge, there is no report to prepare the metal or metal oxide decorated carbonaceous nanosphere by a simple and scalable all-in-one pathway route, which still remains as a significant challenge.

Herein, we have developed a straightforward one-step and versatile hydrothermal method to prepare NiO nanoparticles decorated S-doped hollow carbon nanospheres (SDHCNSs) using a cost-effective and easily available glucose and thiourea as carbon and sulfur precursors respectively. The formation of NiO@SDHCNSs nanoparticles was confirmed by various physical characterizations and used to analyze the glucose level in biological samples without the combination of additional enzyme or mediator. It was found that it exhibits an excellent glucose sensing performance in terms of selectivity, sensitivity, stability, lower detection limit, and linear range of catalytic current due to the hollow architecture of carbon spheres can act as a nanoreactor provides controlled pathways for the NiO nanoparticles and vast surface area to boost their electrocatalytic activity continuously.

2. Materials and methods

2.1. Materials

D-(+)-Glucose, Nickel (II) chloride hexahydrate ($NiCl_2 \cdot 6H_2O$), Sodium hydroxide (NaOH), Isopropyl alcohol (C_3H_8O), Ammonia (NH_3) solution, Thiourea (CH_4N_2S), and Potassium chloride (KCl) were obtained from Sigma-Aldrich (India), Potassium ferrocyanide trihydrate ($K_4Fe(CN)_6 \cdot 3H_2O$), and potassium ferricyanide ($K_3Fe(CN)_6$) were purchased from Himedia-India. Uric acid (UA), L-ascorbic acid (AA), and Dopamine (DA) were purchased from Alfa Aesar-India and were used as-received without any further purification. All other reagents were of analytical grade and doubly distilled water was used throughout the experiment.

2.2. Preparation of sulfur doped hollow carbon nanospheres (SDHCNSs)

We have developed a simple strategy to turn glucose-derived carbon spheres into S-doped activated carbon spheres with a hierarchical hollow structure by introducing sulfur source in the preparation process followed by KOH activation. More interestingly, the S-doped KOH activated carbons spheres are bigger than the undoped one. S-doped hollow carbon nanospheres (SDHCNSs) were prepared through a simple hydrothermal treatment of D-glucose with thiourea and later KOH activation. In a typical synthesis, a homogeneous glucose colourless transparent solution was prepared by dissolving 10 g of glucose monohydrate in 80 mL deionized water by 30 min stirring followed by thiourea sulfur source was added into the above solution at a weight ratio of 1:5 and the as-obtained precursor solution was transferred to 100 mL capacity Teflon-lined stainless steel sealed autoclave and heat treated at 180 °C for 12 h. After the reaction completion, the precipitate was washed with water and ethanol then dried at 80 °C overnight to yield the sulfur-doped carbon nanospheres (SDCNSs). Finally, the SDHCNSs sample was further activated by KOH in the N_2 atmosphere at 650 °C (with a heating rate of 5 °C/min) to obtain the sulfur-doped activated hollow carbon nanospheres (SDHCNSs).

2.3. Synthesis of NiO@SDHCNSs nanocomposite

The as-prepared 50 mg of SDHCNSs were dispersed in 70 mL (1:1) solution of isopropyl alcohol and double distilled water by 30 min sonication, a homogeneous slurry was formed. Then 0.13 g of Nickel chloride hexahydrate (35 mmol) and 0.05 g of HMTA (Hexamethylenetetramine) (70 mmol) were added with the above

slurry and stirred for 2 h at room temperature. The molar ratio of HMTA to $NiCl_2$ was maintained at 2:1 ratio. The above mixture solution was transferred into a 100 mL Teflon-lined stainless steel autoclave and maintained at 160 °C for 10 h and then gradually cooled down to room temperature. After the hydrothermal treatment, the NiO decorated SDHCNSs nanocomposites were collected by centrifugation, washed with water, and ethanol and dried at 80 °C for 6 h in a vacuum oven. In addition, for comparison, pure NiO was also prepared under identical hydrothermal conditions followed as above, without the addition of SDHCNSs.

2.4. Fabrication of NiO@SDHCNSs nanocomposite modified electrodes

To fabricate the NiO@SDHCNSs nanoparticles modified electrode for the glucose sensor, the NiO@SDHCNSs (1 mg in 1 mL) was dispersed in double distilled water by sonication. Meanwhile, a glassy carbon electrode (GCE) with a 3 mm diameter was carefully polished on a polishing cloth with 1.0, 0.3 and 0.05 μm alumina powder and rinsed thoroughly with doubly distilled water. The homogeneous dispersion of NiO@SDHCNSs was drop caste (10 μL) onto the surface of GC electrode and air dried. In addition, carbon nanosphere, S-doped carbon nanosphere, KOH activated SDHCNS and pure NiO modified GC electrodes were also prepared by the above-mentioned process for comparison. The modified GC electrodes were subjected to investigate the electrochemical behaviour of modified electrodes and glucose oxidation.

2.5. Apparatus

The structural and morphological characteristics of SDHCNSs, pure NiO and NiO@SDHCNSs were analyzed by X-ray diffraction (XRD) patterns characterized by using PANalytical X'Pert Pro diffractometer with Cu-Kα radiation (λ = 0.154065 nm) in the angle range of 20–80°. The Raman spectra were recorded for all the samples at room temperature by using Raman spectroscopy (HR800 LabRam, Horiba/Jobin-Yvon) in an excitation wavelength of 532 nm. Morphology of the undoped, doped, activated carbon nanospheres, pure NiO and NiO@SDHCNSs nanocomposite was studied by field emission-scanning electron microscope (FE-SEM) JEOLS-3000H and transmission electron microscopy (TEM) JEM-2010 (HR) instruments. The elemental analysis was carried out with X-ray photoelectron spectroscopy (XPS) AXIS ULTRA DLD at an accelerating voltage of 15 kV. Fourier transform infrared (FT-IR) spectra were recorded for all the synthesized samples for their chemical composition on SHIMADZU FT-IR spectrometer using the KBr pellet method in the range of 400–4000 cm^{-1}.

All the electrochemical characterization was carried out with a conventional three-electrode system using an electrochemical workstation (CHI 6131D, Austin, USA). The modified GC electrodes with the synthesized samples were used as a working electrode; a Pt wire and a saturated calomel electrode (SCE) were served as the counter and reference electrodes respectively. The cyclic voltammetry (CV) and electrochemical impedance spectroscopy (EIS) measurements were carried out by using three electrode system in 0.1 M KCl containing 1.0 mM $[Fe(CN)_6]^{3-/4-}$ redox couple. The cyclic voltammetry measurements were performed in the potential range from −0.2 V to 0.6 V at a scan rate of 50 mV S^{-1}. The EIS measurements were carried out by applying an AC potential of amplitude 5 mV over the DC potential of 250 mV in a frequency range of 100 KHz −100 Hz. For the glucose oxidation, cyclic voltammetry (CV), linear sweep voltammograms (LSV) and amperometry techniques were utilized in 0.1 M NaOH solution using the aforementioned three electrode system. The high pure N_2 gas was purged into the solution for 15 min before the electrochemical test and overflowed to prevent atmospheric O_2 entry into the electrolytic solution during the measurements.

3. Results and discussion

3.1. Structural, composition and morphologies of the SDHCNSs, NiO and NiO@SDHCNSs nanocomposite

The X-ray diffraction (XRD) patterns of the synthesized KOH activated SDHCNSs, bare NiO and NiO-SDHCNSs nanocomposite are shown in Fig. 1 (I) (a), (b) and (c). Bare NiO and NiO decorated SDHCNSs samples exhibits four prominent peaks at the 2θ value of 37.2, 43.2, 62.9 and 75.4, which can be well indexed as (111), (200), (220) and (311) crystal planes of the cubic NiO phase (JCPDS No: 47–1049), respectively. It is noteworthy that no other peaks are identified indicating that the samples have good phase purity. The XRD pattern of NiO@SDHCNSs exhibited a new broad peak centred at 25.3 (2θ) attributed to the (002) plane of graphite. The intensity ratio between the planes (200) and (111) for the bare NiO nanoparticles is 1.69. However, the ratio between the (200) and (111) planes of synthesized NiO@SDHCNSs is 0.55 indicating the growth of NiO is in a particular planes are restricted and thus the intensity of the respective peaks are reduced and consequently their

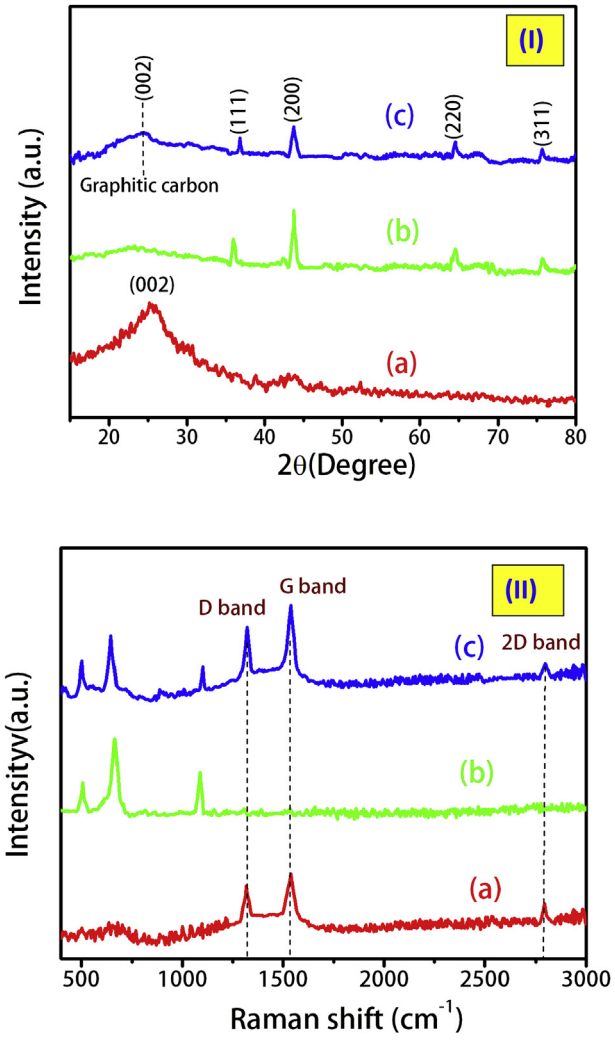

Fig. 1. (I) XRD and (II) Raman spectra of (a) SDHCNSs (b) NiO, and (c) NiO-SDHCNSs nanocomposites.

particles size are dramatically controlled at smallest size [41]. Addition of SDHCNSs makes the diffraction peaks weaker and broader, suggesting the smaller crystallite size of NiO nanoparticles in NiO@SDHCNSs compared with the bare NiO. Thus, the XRD results demonstrate that the NiO homogenously dispersed with uniformly formed sulfur-doped hollow carbon nanospheres. The crystallite size of NiO and NiO@SDHCNSs nanocomposite was ~32 nm and ~58 nm respectively, measured using Scherrer formula [42].

The formation of NiO nanoparticles on the SDHCNSs surface was confirmed by morphological characterization (FESEM and TEM). The formation of hollow structure is quite complicated to resolve the structure of as-prepared nanocomposite because it is questionable to the formation of NiO on the SDHCNSs composite without any external oxidant. However, the formation of nanocomposite probably involves three steps. First, the carbon spheres were formed through dehydration of glucose and subsequently carbonization of the organic compounds. Secondly, Melt-diffusion method was used for sulfur impregnation in the carbon nanosphere to form SDCNs formation. The surface of sulfur-doped carbon nanospheres was achieved by KOH activation. Finally, Ni^{2+} ions were adsorbed onto the surface of activated SDHCNSs through electrostatic interactions and formed NiO. Meanwhile, the slow hydrolysis of HMTA results in the release of OH^- ions into the solution. Thus the Ni^{2+} ions can combine with OH^- ions to form $Ni(OH)_2$. Because of heterogeneous nucleation growth more $Ni(OH)_2$ nanoparticles were deposited on the SDHCNSs. Finally, the $Ni(OH)_2$/SDHCNSs were dried at 120 °C for overnight to convert $Ni(OH)_2$ into NiO and obtained NiO/SDHCNSs hybrid nanostructures [43].

We confirmed that the as-prepared compound is NiO and proposed the possible reaction mechanism for the formation of NiO decorated on SDHCNSs nanocomposite shown below Equations (1)–(4).

$$C_6H_{12}N_4 + 6H_2O \rightarrow 6H_2CO + 4NH_3 \quad (1)$$

$$NH_3 + H_2O \leftrightarrow NH_4^+ + OH^- \quad (2)$$

$$Ni^{2+} + 2OH^- \leftrightarrow Ni(OH)_2 \quad (3)$$

$$Ni(OH)_2 \rightarrow NiO + H_2O \quad (4)$$

The Raman spectrum was used to examine the phase of NiO on the SDHCNSs and also disorders of SDHCNSs was studied through the Raman spectroscopy which is a powerful and non-destructive tool to characterize the carbonaceous materials. Fig. 1 (II) (a), (b), and (c) show the Raman spectrum of KOH activated SDHCNSs, bare NiO and NiO@SDHCNSs nanocomposites, respectively. Three Raman peaks were observed at 506, 663 and 1090 cm^{-1} for bare NiO nanoparticles, which could be attributed to the first-order transverse optical mode (TOM), longitudinal optical mode (LOM) and 2TOM phonon mode of NiO, respectively [44]. The Raman spectra of SDHCNSs exhibits two broad bands at 1319 and 1539 cm^{-1}, the observed peaks correspond to the D (disordered) band arising from a breathing mode of k-point phonons with A_{1g} symmetry and G (graphitic) band arising from the first order scattering of the E_g phonon of sp^2 carbon domains [45]. The D is normally associated with structural defects, an amorphous phase or edges of the carbon that tend to spoil the symmetry. The relative intensity ratio for the D and G bands gives the information about the compounds disorder and crystallinity. Therefore, the intensity ratio of the D vs G band (I_D/I_G ratio) is usually used as a measure for the disordering of the carbon structure and was found to be ~0.93, which exhibits that the NiO@SDHCNSs have a low distortion in hexagonal lattice and also a lower disorder in carbon lattice [46]. We have also observed a small broad 2D peak at 2793 cm^{-1} for SDHCNSs and NiO-SDHCNSs of the graphitic basal plane in carbon sphere with a sufficient number of sp2 carbon atoms. Moreover, the broad bands at 496 and 644 cm^{-1} are corresponding to the NiO phase, which confirms that the NiO is present in the SDHCNSs.

The morphologies of the synthesized carbon spheres, SDCNSs, KOH activated hollow SDCNSs, NiO@SDHCNSs and bare NiO nanoparticles were investigated by field emission scanning (FESEM) and transmission electron microscopy (TEM) analysis. The hydrothermal method has been widely adopted to synthesize the nanoparticles since it is straightforward to apply and has obvious advantages for controlling the size, shape and structure of the nanomaterials. The FESEM images of the synthesized nanospheres are presented in Fig. 2 (a). It is interesting to note that, pure glucose gives rise to interconnected spheres of roughly 0.3 μm in diameter and certain degree of agglomeration have occurred. Moreover, the microsphere was not uniform in size. This may be due to the relatively low hydrothermal temperature [47]. The hydrothermal temperature can significantly influence the particles surrounding environments and determine their size and shapes [48]. Another feature of carbon spheres is that they tend to interconnect with each other. Carbon spheres produced from glucose and fructose tends to form interconnected carbon spheres with a non-uniform size which is reported earlier [49]. On the other hand, the S-impregnated microspheres result in discrete microspheres with considerably increased size and broader size distribution (0.5 μm). Fig. 2(b) and (c) obviously reveal the spheres possess quite rough surfaces this can be attributed to Maillard type reaction [50], where amine group can react with the aldehyde group of the glucose molecule and give rise to variety of products which result in the early formation of nucleation seeds at different points of time resulting larger particle with the heterogeneous size distribution [51]. Transmission electron microscopy analysis was further performed to obtained more information about the specific morphology. Typical TEM images of the samples are shown in Fig. 3 (a). The figure shows that after the KOH activation in the air, the SDCNSs hollows microspheres about 600 nm with a wall thickness 50 nm are obtained. The hollow interior of SDCNSs could also be clearly identified through some small openings on the SDCNSs surfaces (Fig. S1). The morphology of NiO can also be seen from FE-SEM image (Fig. 2 (d)) that reveals the aggregated spherical particles morphology. The size of NiO nanoparticles have been estimated to be around 10–15 nm from TEM analysis (Fig. 3 (C). Finally, the uniform NiO nanoparticles decorated SDHCNSs nanospheres were fabricated via hydrothermal strategy and the corresponding FESEM image (Fig. 2 (e)) and TEM image (Fig. 3 (c)) are present the agglomerated NiO nanoparticles well entrapped within the SDHCNSs. The hollow interior of SDHCNS could also be clearly identified by the sharp contrast between the dark centre and the pale edge in the TEM images of an individual of NiO-SDHCNSs composite Fig. S1. The KOH activation is highly necessary to increase the surface area and create the porosity, and also it helps to form the various surface oxygen functional groups with a rough surface could provide a good scaffold for loading of metal oxide nanoparticles. The synthesized NiO @ SDHCNSs composites are composed of single crystalline inferred from the selected-area electron diffraction (SAED) pattern (Fig. 3 (d)).

In order to analyze the chemical composition, electronic structure and elemental states were also examined by X-ray photoelectron spectroscopy (XPS). As an illustration, Fig. S2 depicts the XPS spectrum of the NiO-SDHCNSs nanocomposite sample, where four peaks 162, 284, 531 and 884 eV are attributed to the presence of S, C, O and Ni. The high resolution-spectra of C 1s spectrum convoluted into four peaks and are shown in Fig. 4 (a), we observed

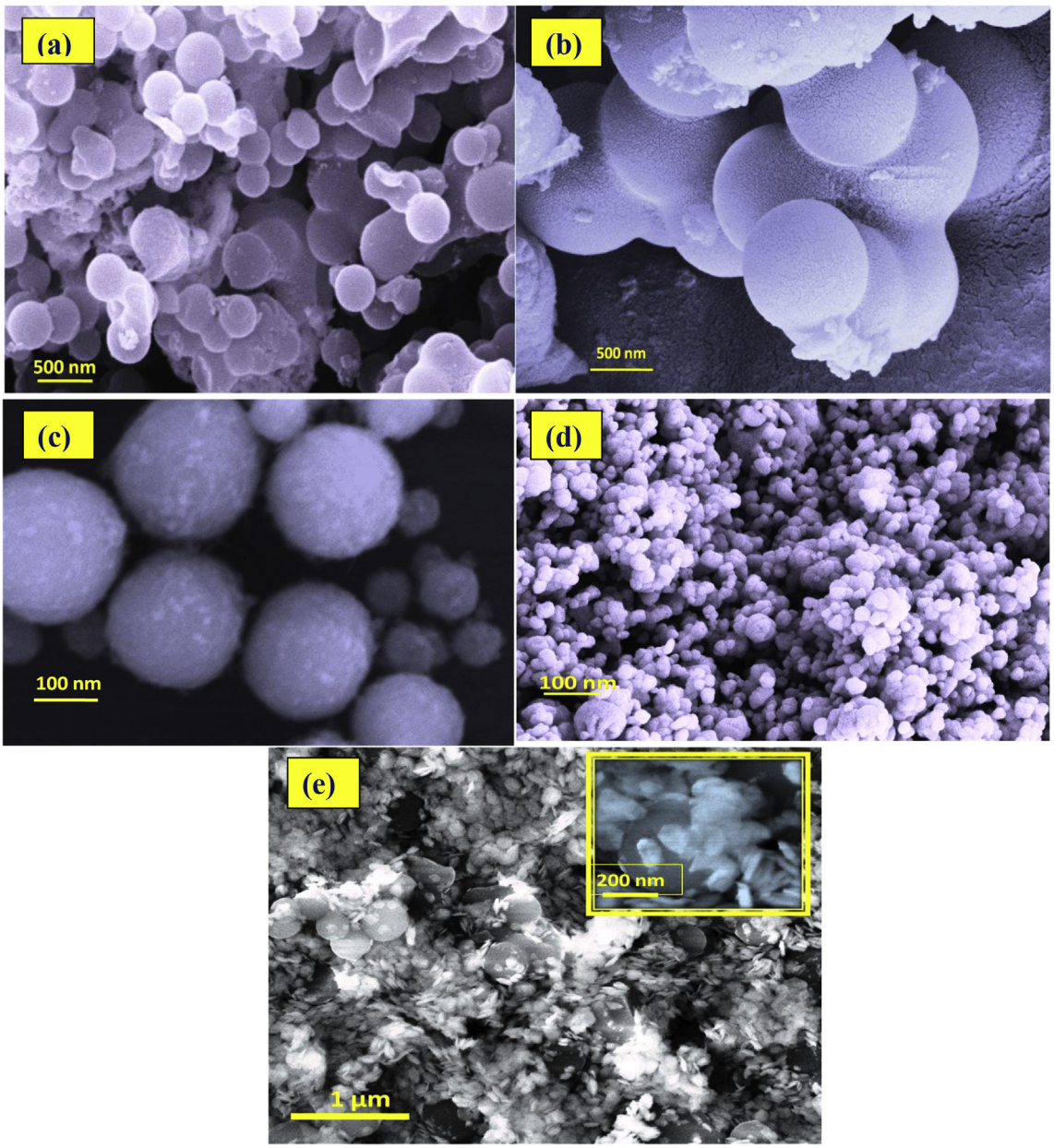

Fig. 2. SEM images of (a) Carbon nanosphers (b) sulfur doped carbon nanosphers (c) KOH activate SDCNSs (d) bare NiO nanoparticles (e) NiO-SDHCNSs nanocomposites.

four peaks at 283.7, 284.2, and 287.4 eV correspond to the C-C, C=O and O-C=O, respectively, these are the typical composition present in carbon lattice [52]. The peak at 285.6 eV is attributed to the C-S, which confirms that the sulfur ion doping on the carbon lattice. Furthermore, sulfur ion doping was confirmed from the high-resolution S 2p spectrum, Fig. 4 (b) displays the peaks at 162.1, 163.4, 164.4 and 168.8 eV for the C-S-C, C=S, C-S=O and sulfate bonding, respectively [53]. To confirm the precise structural composition of NiO embedded SDHCNSs, the high-resolution region on Ni 2p was analyzed and it provides information about the valence distribution and the dispersion of the nickel ions in the NiO core. The XPS patterns of Ni 2p spectra (Fig. 4 (c)) shows two major peak at 856.2 and 876.1 eV correspond to the Ni $2p_{3/2}$ and Ni $2p_{1/2}$, additionally two satellite peaks appeared at 862.1 and 871.6 for Ni $2p_{3/2}$ and Ni $2p_{1/2}$, which is assigned to the Ni (II) ions in the NiO. The spin-energy separation of 19.9 eV indicated the well-defined symmetry of Ni (II) ions in the oxide form [54], which is further confirmed by O 1s spectra (Fig. 4 (d)). The wide scan spectrum of O 1s spectra has four main peaks, where the peaks at 531.1 and 531.6 eV assigned to carbonate structure on the surface. The Gaussian fitted peak at 533.5 eV corresponds to the OH^- group to the adsorbed water molecules at the surface or in C-O. Moreover, 532.8 eV is a typical characteristic peak of C=O or metal-oxygen bonds. The observations confirmed that the as-prepared NiO@SDHCNSs nanocomposites are pure and has related functional groups.

3.2. Electrochemical characteristics of the NiO@SDHCNSs composite modified GC electrode and glucose oxidation

The electrochemical behaviour of the synthesized carbon nanospheres, sulfur-doped carbon nanospheres, alkali-activated S-doped carbon nanospheres, pristine NiO and NiO decorated SDHCNSs were investigated by cyclic voltammetry techniques as it

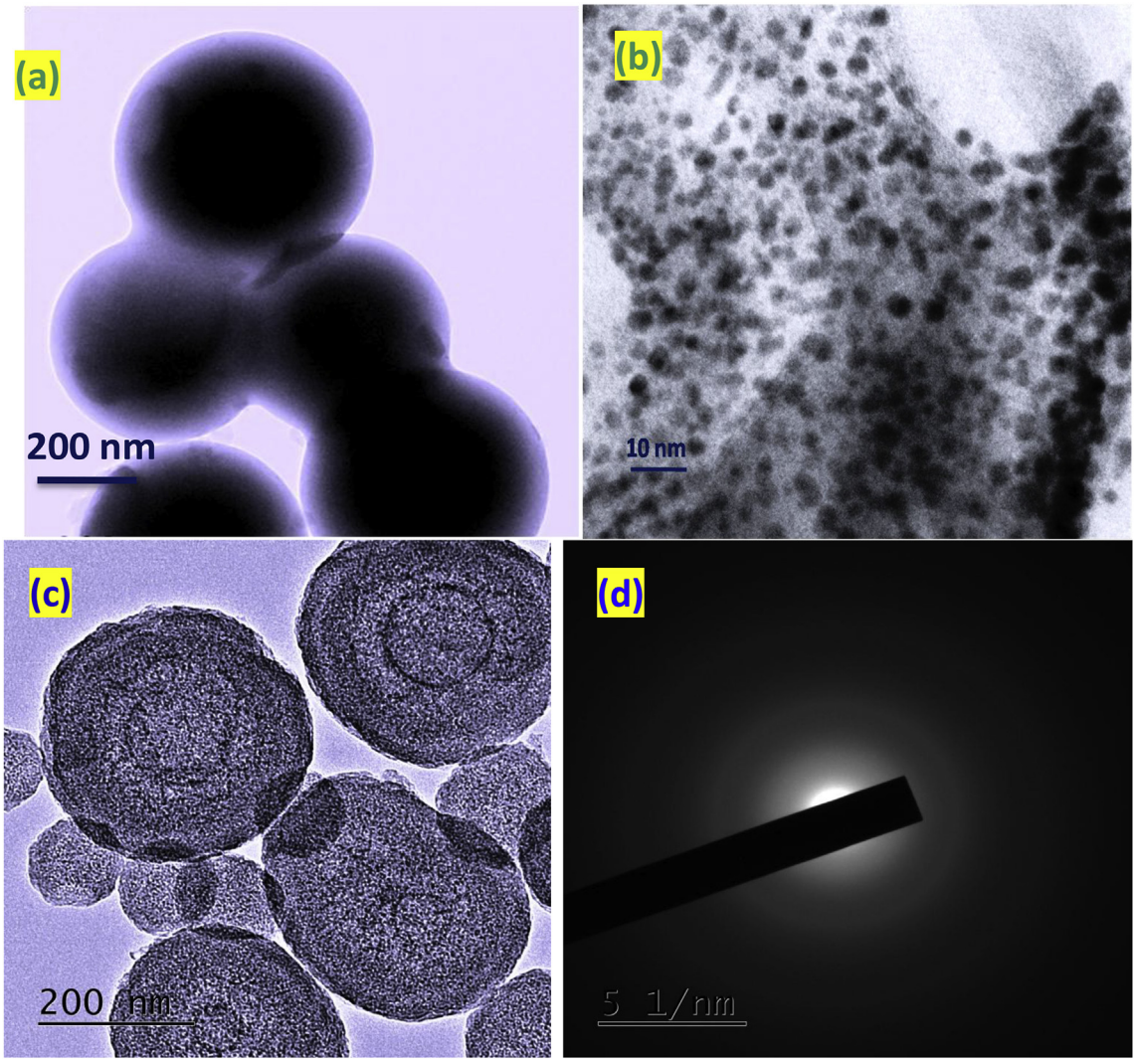

Fig. 3. TEM images of (a) KOH activate SDHCNSs (b) bare NiO nanoparticles (c) NiO-SDHCNSs nanocomposites (d) Selected area electron diffraction (SEAD) pattern of NiO@SDHCNSs nanocomposite.

is considered to be a rapid and reliable tool. Typically, the synthesized samples coated modified glassy carbon electrodes were scanned between the potential of −0.2 V and 0.8 V at a scan rate 50 mV s^{-1} in the presence of 1 mM $[Fe(CN)_6]^{3-/4-}$ in 0.1 M KCl solution and their resulting spectra are presented in Fig. 5 (I). At the bare GCE, the Fe^{3+}/Fe^{2+} redox couple was observed at the potential 0.24 V/0.16 V and the current 1.98×10^{-5} A and 1.96×10^{-5} A was observed for its redox process. However, the carbon nanosphere coated electrode exhibits more sluggish nature of redox couple for the Fe^{3+}/Fe^{2+} with a wide potential difference (ΔEp) of 205mV at reduced peaks currents (Ipa/Ipc) due to its chargeless particle nature of the synthesized carbon nanospheres. In the case of S-doped carbon nanospheres, the negatively charged sulfur with carbon nanospheres enhanced its electrochemical properties by the redox process of Fe^{3+}/Fe^{2+} occurred at 0.21V and 0.098 V with a reduced ΔEp value of 116mV compared to the as-synthesized carbon nanospheres where the ΔEp value is 205mV. Further, the enhanced surface charge of the S-doped carbon spheres by the KOH activation, the very high current at reduced potentials for the oxidation and reduction of iron ions was obtained. It is clearly evident that the surface charge is playing an important role in the redox electrochemical process of a reaction by attracting the ions from the bulk at a large scale. In order to verify the electrochemical characteristics of the nanostructured NiO nanospheres at 10—15 nm size were employed alone and decorated on the SDHCNSs. At the NiO@SDHCNSs electrode a well defined two pairs of redox couples are observed pertaining to the redox process of $Ni^{2+}/^{3+}$ in the electrode and Fe^{3+}/Fe^{2+} present in the solution at 0.608 V/0.587 V and 0.505 V/0.432 V, respectively. The NiO nanospheres exhibit the redox process for the $Fe^{3+}/^{2+}$ and $Ni^{2+}/^{3+}$ at the potential of 0.34 V/0.065 V and 0.608 V/0.587 V, respectively. However, the redox peaks on the NiO are not well defined, they are mostly sluggish in nature and the peak current values are very minimum when compared to the NiO@SDHCNSs electrode, where $Fe^{3+}/^{2+}$ redox process shows a 168% and 11 times higher anodic and cathodic peak currents even though the process takes place at the higher potentials. For the $Ni^{2+}/^{3+}$ system the anodic peak potential is not changed but only a 17 mV lowered for the $Ni^{3+}/^{2+}$ whereas, the peaks currents were enormously increased to 4.77×10^{-5} A and 3.95×10^{-5} A from 2.53×10^{-5} A and 2.89×10^{-5} A for the $Ni^{2+}/^{3+}$ (anodic peak) and $Ni^{3+}/^{2+}$ (cathodic peak), respectively. These results clearly indicate that the newly formed NiO@SDHCNSs hybrid nanocomposites have newer functionalities, which are different from pure NiO and SDHCNSs counterparts. This could be attributed

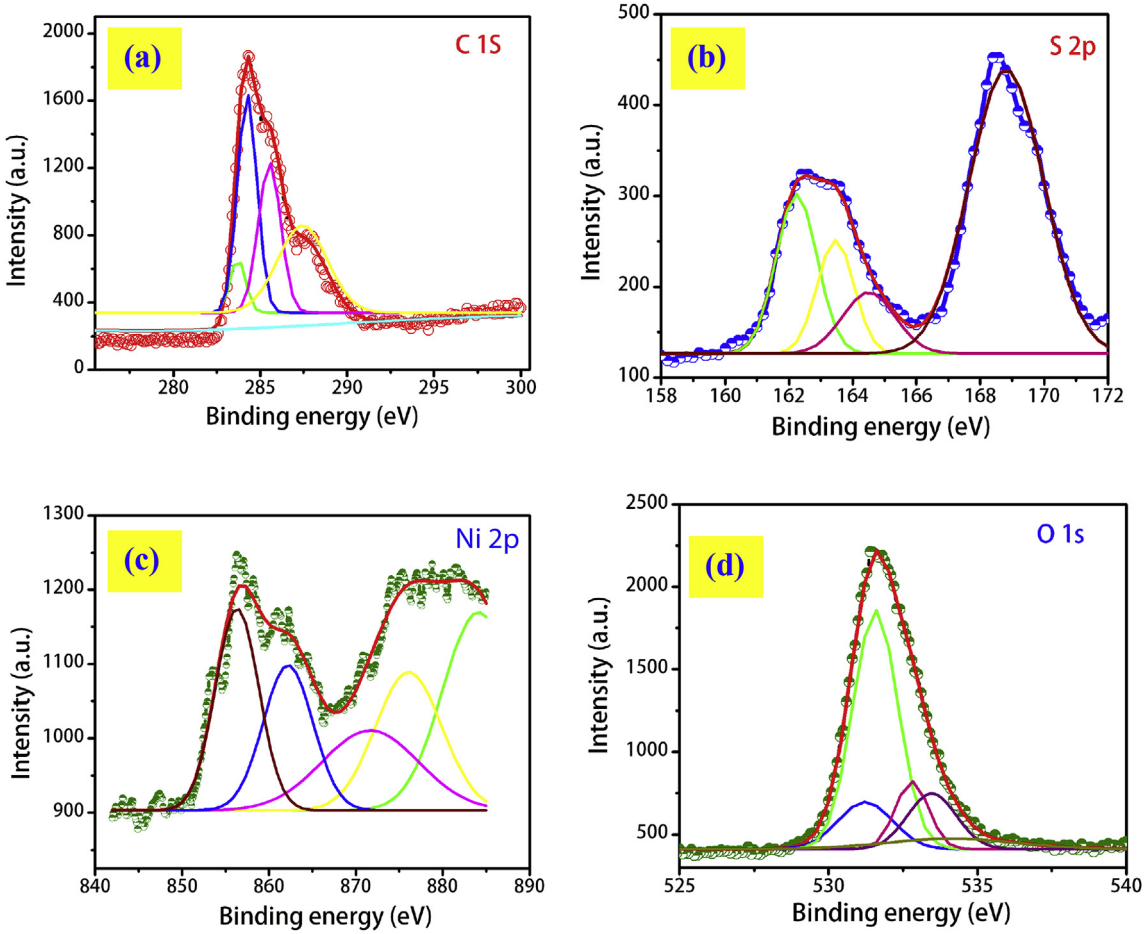

Fig. 4. XPS core level spectra of C 1s, S 2p, Ni 2p and O 1s of NiO-SDHCNSs hybrid nanocomposite.

to the hollow sphere like structure with the high surface area and good electrical conductivity of the NiO@SDHCNSs hybrid nanocomposite, which allow the diffusion of more $[Fe(CN)_6]^{3-/4-}$ redox couple on its surface [3].

The CV behaviour of NiO@SDHCNSs modified electrode at different scan rates (10–150 mV s^{-1}) was further investigated in 0.1 M KCl solution containing 1 mM $[Fe(CN)_6]^{3-/4-}$ as redox probe and presented in Fig. 5 (II). It can be seen that the peak currents of $[Fe(CN)_6]^{3-/4-}$ redox process were increased with increasing the scan rate from 10 to 150 mV s^{-1}. Further, a good linearity was obtained while plotting the current against the square root of the scan rate (Fig. 5 (III)) with the high linear coefficient of 0.997 for both Ipa and Ipc, indicating the diffusion controlled electrochemical kinetics with a fast electron transfer rate. The slope of the plot of log (Ip) Vs. log (V) (Fig. S3) is 0.98 with a correlation coefficient of 0.998, which is close to the theoretical slope of 1 for thin layer voltammetry [55]. The surface concentration of the electroactive species has been estimated from the Ip vs. V plot and according to the Brown-Anson equation

$$Ip = n^2F^2I^*AV/4RT$$

Where, n is the number of electrons transferred, F is the Faraday constant (96,485 mol^{-1}), I^* is the surface concentration (mol cm^{-2}), A is the surface area of the working electrode (0.07 cm^2), V is the scan rate (50 mV s^{-1}), R is the gas constant (8.314 J mol^{-1} K^{-1}) and T is the absolute temperature (298 K). The average surface concentration (I^*) of the pristine SDHCNSs and NiO@SDHCNSs modified electrodes have been estimated as 3.61×10^{-9} mol cm^{-2} and 2.12×10^{-9} mol cm^{-2} respectively, it suggests that the particle size of NiO@SDHCNSs is higher compared to that of pure SDHCNSs which is in good agreement with the average particle size calculated from the XRD data and observed from the FESEM/TEM images. On the other hand, the anodic peak potentials shifted towards positive direction and the cathodic peak potentials shifted to the negative direction at higher scan rates, which resulted increasing the peak separation between the anodic and cathodic peak. The peak separation at higher scan rate could be attributed to the heterogeneous electron transfer kinetics indicating a quasi-reversible redox process.

In addition, we have performed the electrochemical impedance spectroscopy (EIS) experiments to analyze the electrochemical kinetics at the electrode/electrolyte interface. The obtained Nyquist plot for bare GCE, SDCNSs, KOH activated SDCNSs, pure NiO and NiO@SDHCNSs modified GC electrodes are presented in Fig. 5 (IV). The impedance spectra consists a semicircle portion in the high and medium frequency region accompanied by the linear portion in the lower frequency region. As known, non-zero interrupted resistance before the semicircle in the high-frequency region denotes the equivalent serious resistance (ESR), and it is a contribution of solution resistance and intrinsic resistance of the active material. The charge transport process of the modified electrode was studied by monitoring charge transfer resistance (R_{CT}) at electrode/electrolyte interface, where the well-defined semicircle was obtained. The value of charge-transfer resistance for bare GCE, SDCNSs, KOH-SDCNSs, pure NiO and NiO@SDHCNSs modified electrode was

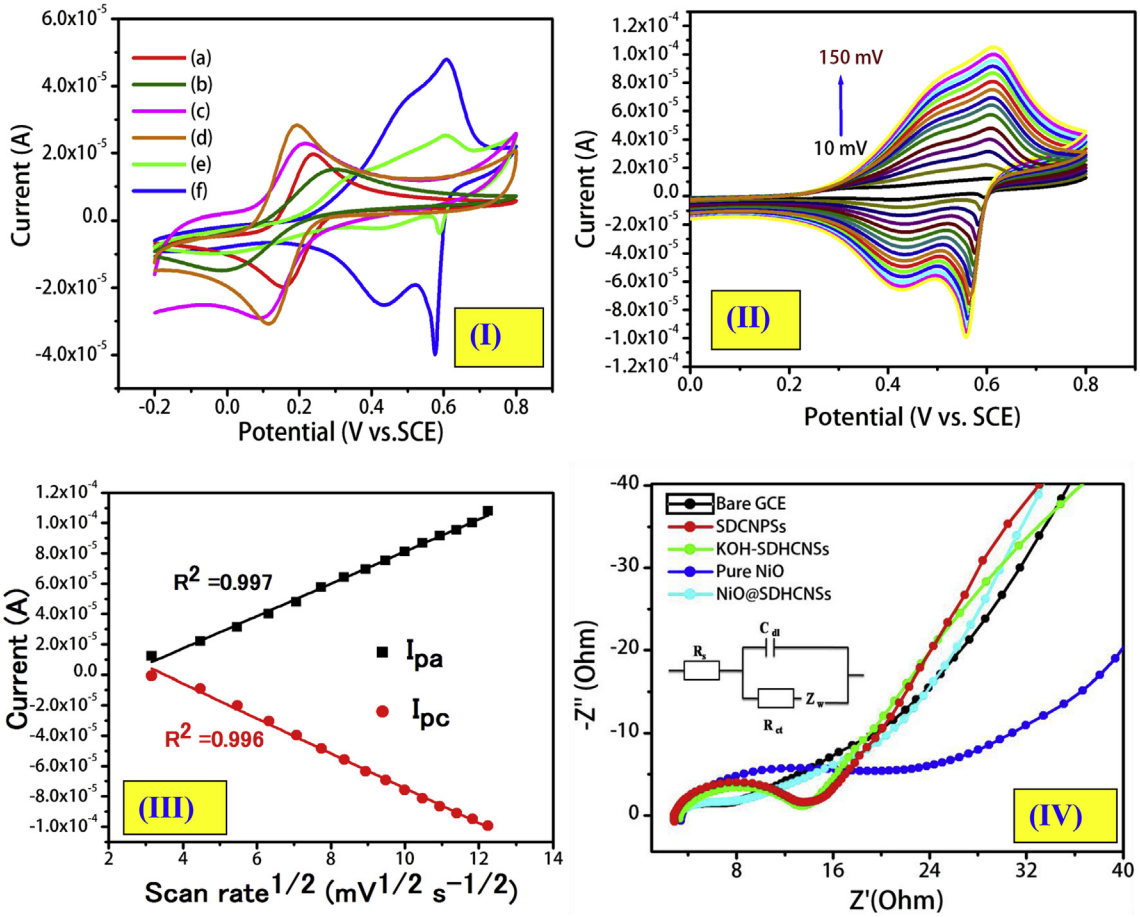

Fig. 5. (I) CV behaviour of (a) Bare GC, (b) Pure carbon sphere (c) S-doped carbon nanosphere (d) KOH activated SDHCNSs (e) pure NiO and (f) NiO@SDHCNSs in the presence of 1 mM $[Fe(CN)_6]^{3-/4-}$ in 0.1 M KCl at scan rate of 50 mV s^{-1} (II) CV recorded at 10–150 mV s^{-1} with a step value of 10 mV s^{-1} for NiO@SDHCNSs in the presence of 1 mM $[Fe(CN)_6]^{3-/4-}$ in 0.1 M KCl, (III) The calibration plots of peak current vs. square root of scan rate, (IV) Nyquist plots of bare GCE, SDCNPSs, KOH activate SDCNPSs, pure NiO and NiO@SDHCNPSs measured in the frequency range from 100 kHz to 1 Hz in the presence of 1 mM $[Fe(CN)_6]^{3-/4-}$ in 0.1 M KCl solution.

estimated to be 7.3, 15.6, 12.3, 21 and 8.2 Ω cm^{-2}, respectively. Compared with the pure NiO and SDHCNSs modified GC electrode, the charge-transfer resistance of the NiO@SDHCNSs/GCE in ferrocyanide redox couple is 2.5 and 1.5 fold lower than that of pristine samples respectively, indicating the good electronic conductivity of the NiO@SDHCNSs nanocomposite. These results are in good agreement with the peak current (Ipa) values obtained from CVs measurements. Thus, it is indicate that the NiO@SDHCNSs modified electrode possesses a high electrical conductivity and electron transfer rate. Hence, we have used NiO@SDHCNSs modified GC electrode for further investigations.

To investigate the electrochemical determination of glucose, we have carried out cyclic voltammetric technique using the synthesized pure NiO, SDHCNSs and NiO@SDHCNSs modified GCE in 0.1 M NaOH electrolyte at a scan rate of 50 mV s^{-1}, obtained CV with and without the presence of 5×10^{-4} M glucose in the potential range of 0.0–0.6 V are shown in Fig. 6 (I) and (II). Here, NiO@SDHCNSs/GCE reveals a couple of well-defined redox-peaks at 0.46 and 0.35 V, could be attributed to the redox reaction of Ni (III)/Ni (II) couple on the electrode surface representing the formation of NiOOH and $Ni(OH)_2$, respectively on the solid surface of the NiO@SDHCNSs electrode in the NaOH electrolyte. The deposition of the Ni^{2+}/Ni^{3+} redox couple was confirmed by the continuous increment of the anodic and cathodic peak currents during the successive CV scan, which is in agreement with the previous studies [26]. The overall reaction mechanism is suggested below.

$$NiO + OH^- \rightarrow NiOOH + e^- \quad (5)$$

$$Ni(OH)_2 + OH^- \leftrightarrow NiOOH + H_2O + e^- \quad (6)$$

The redox couple (Ni^{2+}/Ni^{3+}) of NiO@SDHCNSs/GCE shows the peak separation (ΔEp) of 85 mV only, whereas the pure NiO/GCE shows (ΔEp) 103 mV. The lower peak separation and higher peak current response of NiO@SDHCNSs suggest the highly reversible redox couple through the faster electron transfer through the SDHCNSs is feasible when compared with pure NiO/GCE. In addition, the electrochemical behaviour of bare GCE and SDHCNSs/GCE was also evaluated for comparison, which shows no peaks in that potential window and provides low background current.

In order to better understand the electrocatalytic properties of the developed non-enzymatic sensor GCE, SDHCNS, pure NiO and NiO@SDHCNSs for glucose oxidation, cyclic voltammetric measurements were carried out in 0.1 M NaOH electrolyte containing 500 μM glucose at a scan rate of 50 mV s^{-1} shown in Fig. 6 (II). The bare GCE and SDHCNSs/GCE show inconspicuous redox peak in the working potential range with glucose (Inset Fig. 6 (II)). On the other hand, the anodic peak current (Ipa) was greatly (3.5-fold) improved from 1.8×10^{-4} to 6.6×10^{-4} A when the NiO@SDHCNSs hybrid nanocomposite modified electrode was employed to glucose

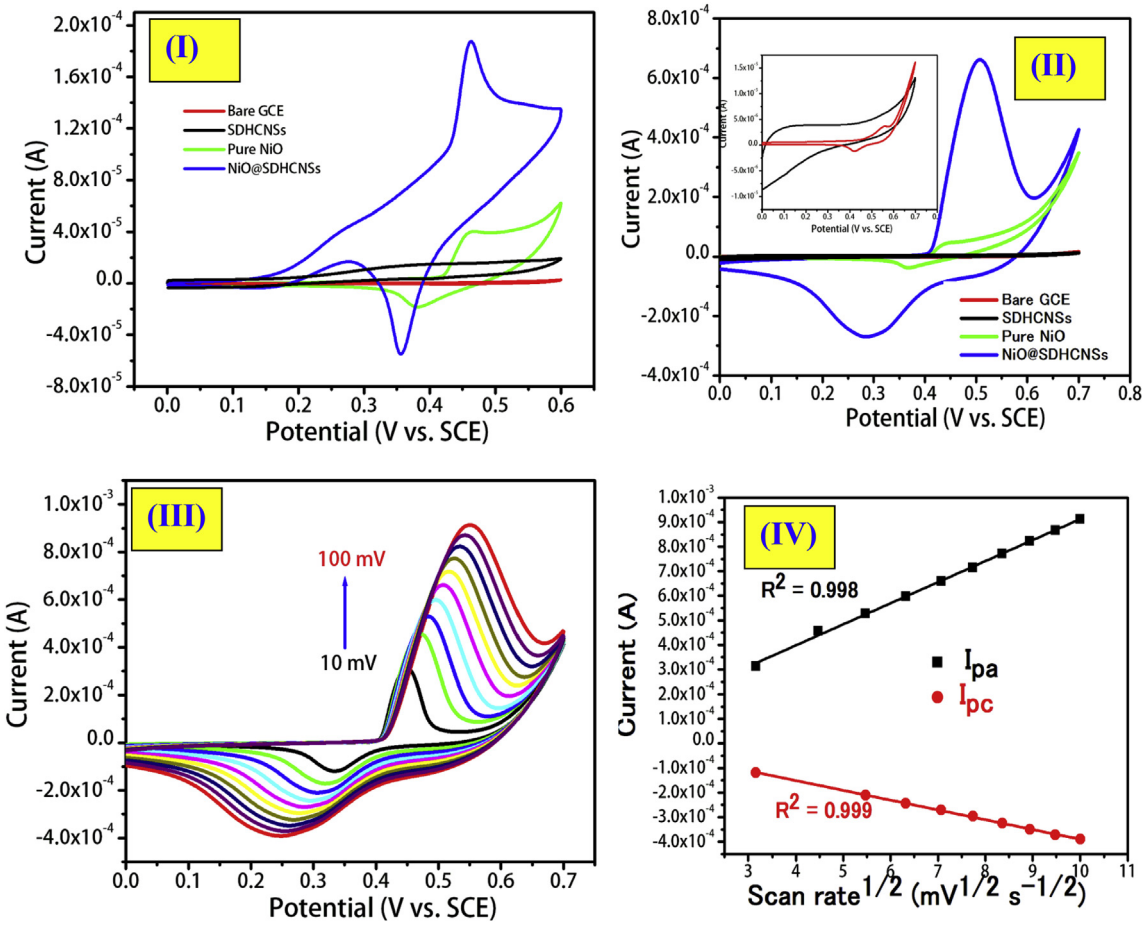

Fig. 6. Cyclic behaviour of (a) Bare GC, (b) SDHCNSs (c) NiO (d) NiO@SDHCNSs without (I) and with (II) 500 μM Glucose in 0.1 M NaOH solution at a scan rate of 50 mV s^{-1}, (III) CV behaviour of NiO@SDHCNSs modified electrode at scan rate of 10–100 mV s^{-1} with a step value of 10 mV s^{-1} in 0.1 M NaOH solution containing 500 μM Glucose and (IV) The calibration plots of peak current vs. square root of scan rate.

sensing. This is attributed to the synergetic effect, fast molecular diffusion, rapid electron transfer rate and the existence of more active sites on the NiO@SDHCNSs hybrid nanocomposite and the catalytic mechanism is as follow.

$$NiOOH + glucose \rightarrow Ni(OH)_2 + glucolactone \quad (7)$$

This phenomenon implies that the oxidation of glucose to gluconolactone at the NiO@SDHCNSs/GCE is electrocatalyzed by the $Ni(OH)_2$/NiOOH redox couple which is generated on the surface of NiO@SDHCNSs during the CV process in the alkaline medium as showed in Equations (5)–(7). This excellent electrocatalytic ability is due to the rich production of NiOOH layer generated on the surface of NiO@SDHCNSs/GCE. The reason for the notable electrocatalysis towards glucose at NiO@SDHCNSs/GCE modified electrode is may be deduced as the SDHCNS provides an excellent matrix supported to the Ni^{2+} ion adsorption by its heteroatoms (S and O), where the electron clouds on the heteroatoms can interact with the d-orbital of nickel ions and make the nickel ions soften and adsorb on the carbon sphere surface which helps to oxidize the Ni^{2+} into $Ni(OH)_2$ on the electrode surface. However, the glucose oxidation at pure NiO/GCE electrode was examined in the presence of 500 μM glucose reveals that the electrocatalytic peak current is lower than on NiO@SDHCNSs/GCE (Fig. 6 (II)). This study confirms that the synthesized NiO@SDHCNSs shows higher performance compared to the pure NiO spherical exerted the enhanced surface area and special morphological nature of the hybrid composites.

Further, the effect of scan rate (10–100 mV s^{-1}) on the electrocatalytic oxidation of glucose (5×10^{-4} M) at the NiO@SDHCNSs/GCE modified electrode was investigated. When increasing the scan rates, the Epa was shifted towards the positive direction and the Epc moved towards the negative potential as shown in Fig. 6 (III). As it is seen, reduction/oxidation peak current of glucose enhanced remarkably with increasing the scan rates. This result suggests that the electrocatalytic glucose oxidation is higher due to the increased charge-transfer kinetics of NiO@SDHCNSs/GCE. The ratio of Ipa/Ipc was above the unity; it indicates that the Ni^{2+}/Ni^{3+} hydrous oxide transformation process is a quasi-reversible reaction [56]. At this point, it is worth mentioning due to the charge interaction between the positively charged Ni, Na and negatively charged OH^- ion in the environment [57]. In addition, peak currents Ipa and Ipc of the glucose oxidation were plotted against the square root of the scan rate shown in Fig. 6 (IV) reveals that the good linearity with the correlation coefficient of 0.999 and 0.999 for Ipa and Ipc respectively. These values reveal that the glucose oxidation at NiO@SDHCNSS/GCE is a highly diffusion controlled process. This is because of the diffusion transport of OH^- ions from the electrolyte (liquid) to the electrode surface (solid) via diffusion ↔ adsorption vice versa during the reaction as shown in Equation (8) [58].

$$^{2+}Ni(OH)_{2(solid\ surface)} + OH^{-}_{(Liquid\ phase)} \times \underset{Adsorption\ process}{\overset{Diffusion\ process}{\longleftrightarrow}} {}^{3-}NiOOH_{(solid\ surface)} + e^{-} \quad (8)$$

The oxidation of glucose in the alkaline solution is to be demonstrated that chemisorptions followed by dehydration steps to form gluconolactone through the intermediate formation. The dehydrated glucose intermediate adsorbed on the NiO@SDHCNSs electrode surface oxidized to form gluconolactone during the positive potential scan. Initially, more weakly adsorbed gluconate is formed, further increasing the potential at positive scan the adsorbed dehydrogenated intermediate is oxidized to form glucono-lactone without the cleavage of the C-O-C band, which is slowly desorbed from the nanospheres towards bulk whereby the surface of the electrode is regenerated. The multivalent nickel oxide redox couple is responsible for the electrocatalytic oxidation of glucose. Usually, electro-oxidation of organic molecules at NiOOH involves the reaction of trapped hydroxyl radicals on the nickel surface. The direct electrocatalytic glucose oxidation deemed at nickel oxyhydroxide is the abstraction of a hydrogen atom at the C1 atom. At the initial state, the $Ni(OH)_2$ is electro-oxidized within the alkaline medium to produce catalytically active NiOOH species as shown in equation (6). After the formation of the Ni(III) species, the adsorbed glucose by the electrode surface undergoes hydrogen abstraction at the C1 atom of glucose molecules at the electrode surface to form a radical intermediate species and reforming the $Ni(OH)_2$ species as shown in equation (7). Finally, the hydroxyl anions in the electrolyte solution rapidly complete the oxidation of the organic radical intermediate species to form gluconolactone. This result in the release of an electron which concurrently responsible for the large anodic peak current and oxidation of glucose at the same time gets de-oxidized to Ni^{2+} as shown in equation (8). The anodic peak current is increased with increasing the concentration of glucose. The adsorption of the intermediate is not confirmed however, as the bulk oxidation of glucose seems to occur rather than surface constrained oxidation, as shown by the linear proportionality of peak current to square root of scan rate. Such a phenomenon of an excellent electrochemical response could be attributed to the hollow spheres and high surface area possessed by as-synthesized NiO@SDHCNSs nanostructures. In order to get information of the charge transfer coefficient (α) and the number of electrons involved in the rate-determining (n_α), a Tafel plot of Ep Vs. *log I* was drawn (Fig. S4) using the data from the rising part of the current-voltage curve obtained at different scan rates from 10 mV S^{-1} to 100 mV S^{-1} for 500 μM glucose concentration. The calculated Tafel slope from the plot was 182 mV/dec (±3 mV) for the NiO@SDHCNSs/GCE electrode. These results indicate that the oxidation of glucose is a one-electron controlled process (see Eq. (7)) that would be the rate determining/limiting step and the charge transfer coefficient was calculated to be $\alpha = 0.59$.

Fig. 7 shows the LSV (linear sweep voltammograms) response of glucose (10–100 μM) on NiO@SDHCNSs hybrid nanocomposite modified electrode with successive addition of 10 μM glucose solution to 0.1 M NaOH solution at a scan rate of 50 mV s^{-1}. The peak potential for the electrocatalytic oxidation of glucose is increased positively with increasing the concentration of glucose. Further, there is a linear relationship between the peak current and glucose concentration with a correlation coefficient of 0.999 (Fig. 7 inset) and this confirms that the oxidation of glucose is diffusion controlled, which is in good agreement with an earlier report [59]. To further investigate the enzyme-free glucose oxidation, we have employed DPV (Differential pulse voltammetry) for glucose concentration from 0 to 10.0 μM with a step value of 1 μM at the voltage range from 0.0 V to 1.0 V in 0.1 M NaOH solution and the resulting spectra are presented in figure S5 (I). It is clear that an obvious increase in the oxidation peak current was observed for the increased glucose concentration. The calibration plot obtained from the DPV measurements is presented in Figure S5 (II). The results indicate that the NiO@SDHCNSs/GCE modified electrode exhibits an excellent electrocatalytic activity towards the glucose oxidation in the glucose concentration of interest between 1.0 and 10.0 μM. Moreover, for all the glucose addition (1.0–10.0 μM) exhibits well-defined oxidation peak at 0.55 V can be observed which is well corroborated with our CV and amperometric results. The linearity between the concentration and the peak currents exhibits ΔIp (A) = 0.66 ± 3 with a correlation coefficient (R^2) of 0.999. This can be attributed to the NiO nanoparticles decorated on heteroatoms-enriched activated carbon nanospheres, which significantly facilitates the transport of electrons and nil electrode fouling due to oxidized glucose at electrolyte/electrode interface consequently insulation free active surfaces intact with more analyte molecules for further redox process. Therefore, a wide range of glucose concentration with high correlation coefficient was confirmed once again with the modified NiO@SDHCNSs/GCE electrodes.

3.3. Effect of applied potential and electrolyte concentrations

Prior to the non-enzymatic glucose sensor, experimental parameters influencing the analytical performance of the fabricated NiO@SDHCNSs/GCE modified electrode were optimized. It is well known that the applied potential strongly affects the amperometric response of biosensors. Therefore, the effect of applied potential was first studied on the Amperometric response of glucose on the NiO@SDHCNSs/GCE hybrid electrode. In order that constant potential chronoamperometry was performed in the potential range of 0.2–0.6 V with the drop wise addition of 1 mM glucose in 0.1 M NaOH solution under stirred condition (Fig. S6). Obviously, the modest current is observed in the potential range of 0.2–0.4 V and increasing significantly from 0.4 to 0.55 V. Compared with at 0.55 V, the current response decreases at 0.6 V and also the background current and the noise increase greatly. Considering the maximum current response for the oxidation of glucose at 0.55 V was selected as an optimum applied potential for amperometric detection of glucose in the subsequent studies.

In most cases, the electrolyte concentration is an important factor in the electrochemical reaction. In non-enzymatic glucose sensors, the alkaline medium may be favourable to improve the electrocatalytic activity of the proposed modified electrode. Hence, the impact of NaOH concentration (0.025–0.2 M) was investigated by CV at NiO@SDHCNSs between 0.0 V and 0.7 V in the presence of 500 μM glucose at 50 mV s^{-1} are shown in Fig. 8. The anodic peak current was increased correspondingly when the electrolyte concentration increased to 0.1 M. This is because of the huge availability of OH^- ions and improved electrocatalytic activity of NiO@SDHCNSs on the glucose oxidation. However, further increasing the electrolyte concentration, the peak current is decreased. The possible reason could be that too much of OH^- ions on the surface of catalysts act as a barrier for glucose to reach the catalytic surface of the electrode result in a decreased current signal.

3.4. Amperometric determination of glucose at NiO@SDHCNSs/GCE

The amperometric analysis is an extremely attractive electrochemical technique to evaluate the high sensitivity, selectivity and lower detection limit towards glucose oxidation. Under the above-optimized conditions, the amperometric study was carried at NiO@SDHCNSs/GCE with the successive step-wise addition of different concentration (1 μM- 13 mM) of glucose in 0.1 M NaOH at

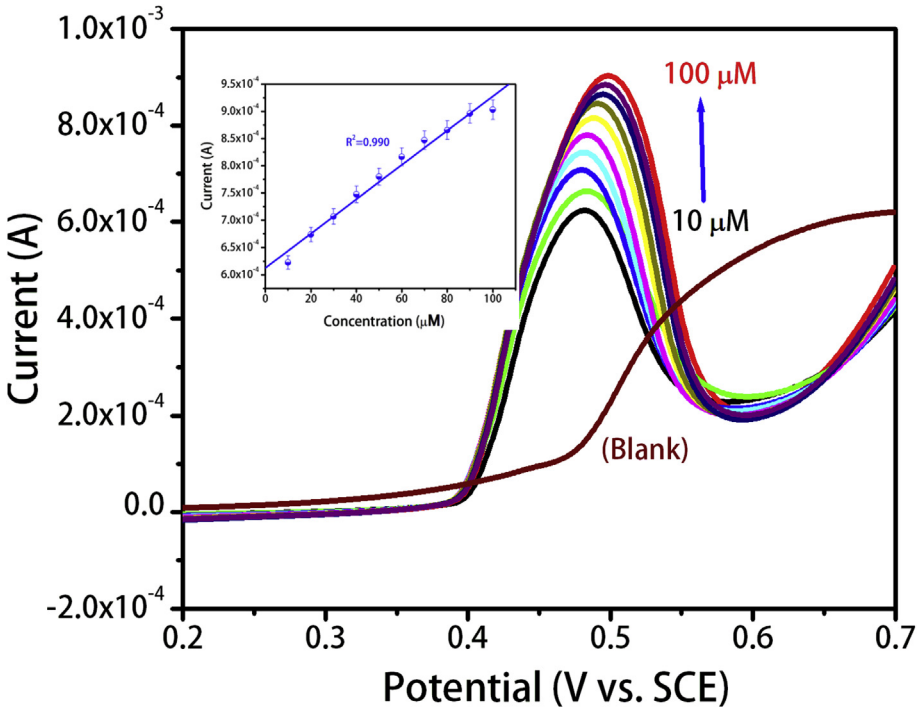

Fig. 7. LSV obtained for glucose in the concentrations ranging from 10 to 100 μM. Glucose was added in steps of 10 μM each at the NiO@SDHCNSs modified electrode in 0.1 M NaOH and inset shows the linearity plot of current vs. concentration.

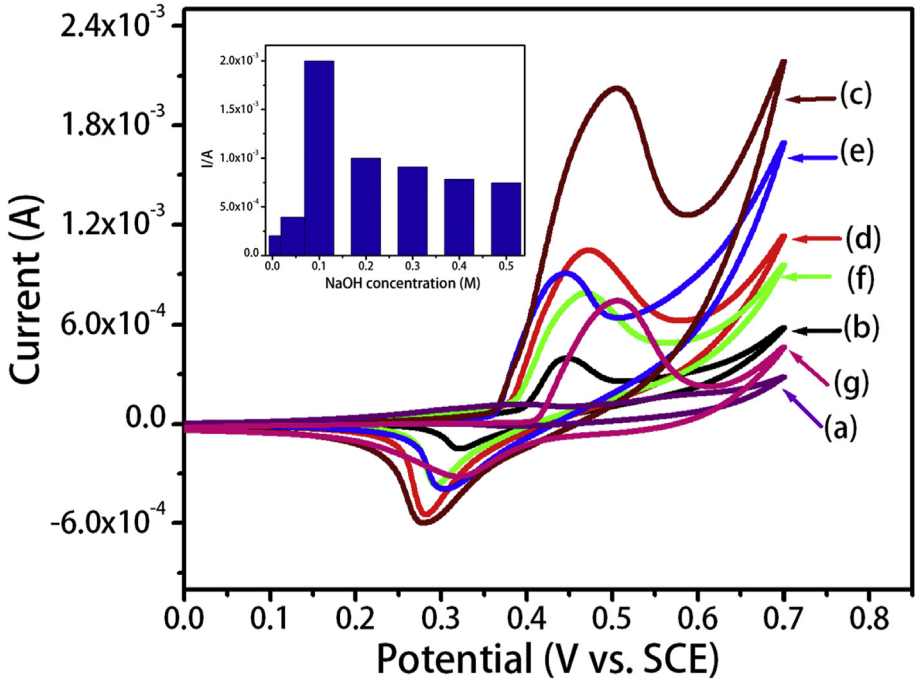

Fig. 8. CVs of NiO@SDHCNSs modified electrode towards 500uM glucose at 50 mV s^{-1} under different NaOH concentrations (a–g) 0.025 M, 0.05 M, 0.1 M, 0.2 M, 0.3 M, 0.4 M and 0.5 M, Inset shows plot of oxidation peak current of glucose vs. electrolyte concentration.

0.55 V vs. SCE and shown in Fig. 9 (I), where the different concentration of glucose was added at a 50 s time interval into the alkaline medium, a rapid current increment was observed. It is found that the NiO@SDHCNSs/GCE modified electrode reveals good electrocatalytic responds quickly with an increase of glucose concentration and reveals a steady-state signal within 5 s demonstrating the excellent electrocatalytic activity, number of active sites, good electron mobility properties of the hybrid nanocomposite glucose electro-oxidation. The resultant current response was plotted against the concentration of glucose and shown in Fig. 9 (II). The calibration curve of the electrochemical response of NiO@SDHCNSs/GCE shows the linear concentration range from

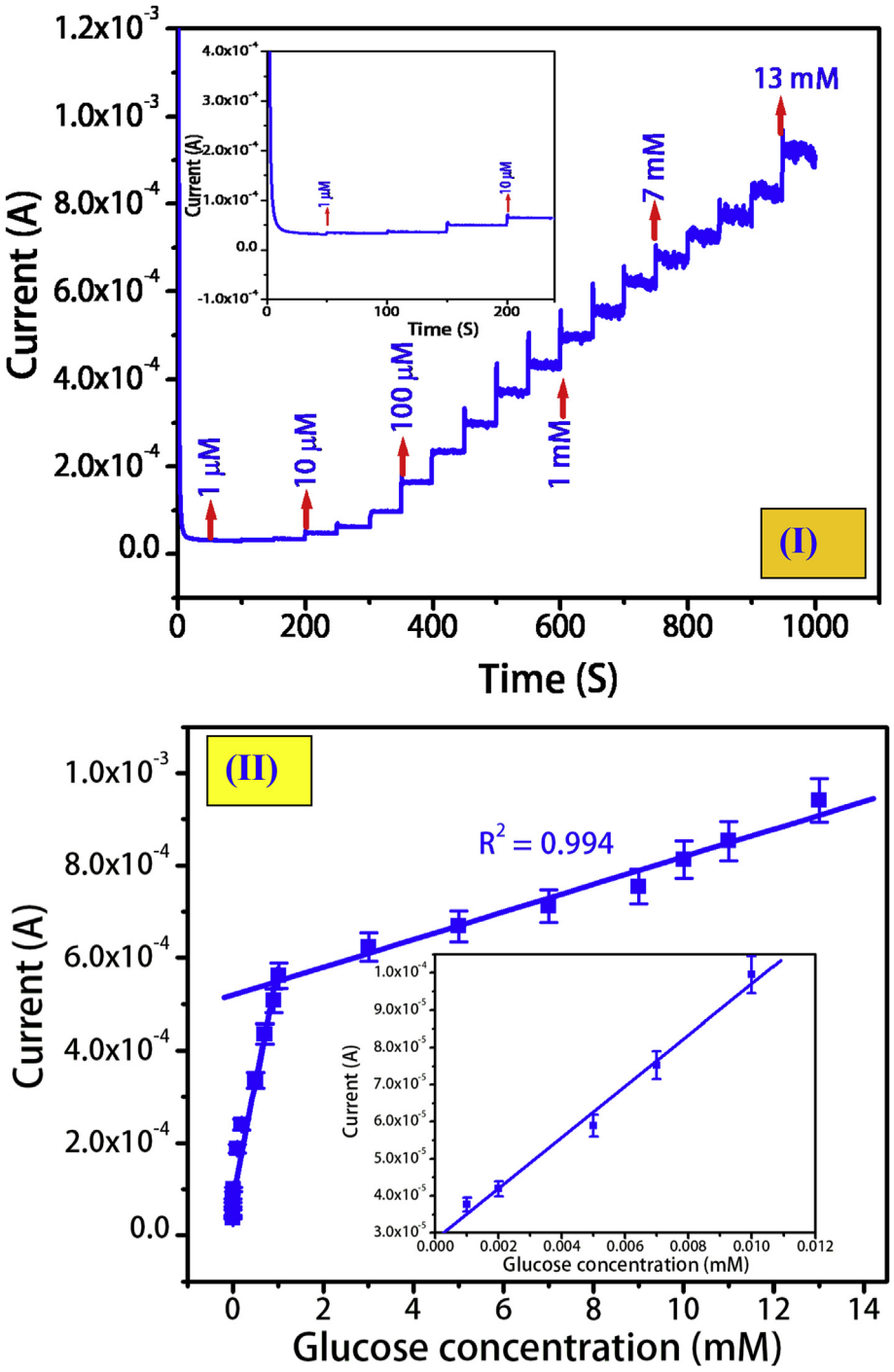

Fig. 9. (I) Amperometric response of NiO@SDHCNSs modified GCE in 0.1 M NaOH with different concentration of glucose (1 μM –13 mM) applied potential +0.55 V and inset shows the enlarged view of the micromolar detection of glucose (II) corresponding calibration curves for current vs. concentration of glucose.

0.001 to 1.00 mM with a high correlation coefficient of 0.994. However, in higher concentration (1.00–13.00 mM) the second linear range was observed with a correlation coefficient of 0.996. When the concentration of glucose is above 13.00 mM, the current response was decreased gradually, it may be due to the diffusion dominance and adsorption of glucose ions onto the electrode surface which is partially covered by the adsorbed reaction intermediates cannot offer sufficient sites to accommodate the incoming glucose [60]. Significantly, NiO@SDHCNSs/GCE manifests a good linearity even at a low concentration range from 1.0 to 100 μM and the correlation coefficient of 0.998. From this low linear range, we have calculated the limit of detection (LOD) was 0.52 μM (S/N = 3) and the sensitivity of the sensor 1697 μA mM^{-1} cm^{-2}. The detection performance of the fabricated modified electrode is compared with other reported NiO based non-enzymatic glucose sensors. As shown in Table 1 [61–71], it is worth mentioning that the NiO@SDHCNSs modified electrode exhibits prominent electrocatalytic performance for glucose sensing in terms of the ultra-high sensitivity, the lower detection limit and wide linear range.

Table 1
Comparison of the performance of fabricated Non-enzymatic NiO@SDHCNSs glucose sensor with other Nickel based Non-enzymatic glucose sensor.

Electrode	Detection limit (μM)	Linear range (mM)	Sensitivity (μA $mM^{-1}cm^{-2}$)	Ref
NiNWs	0.07	0.0005–4	1043	[17]
$Ni(OH)_2$/CILE	6	0.05–23	202	[22]
NiCFs	1	0.002–2.5	420.4	[30]
Ni@f-MWCNT/GCE	0.17	0.1–12	2477	[61]
3D NF-G-NiO	10	0.01–0.2	3230	[62]
NiO/C/GCE	2	0.002–1.279	301900	[63]
$Ni(OH)_2$@PPy NW	0.3	0.001–3.86	1043	[64]
$Ni(OH)_2$/C NC	0.14	0.001–15	1006.4	[65]
Ni-PANI-rGO/GCE	0.08	0.0001–1.0	6050	[66]
PVP/GNs/NiNPs/CS/GCE	0.03	0.0001–0.5	103.8	[67]
NiO-HSs@RGO-NT	0.03	0.0006246–10.50	3796	[68]
Ni-MOF/Ni/NiO/C	0.8	0.004–5.56	367.45	[69]
HAC/NiO	1	0.01–3.3		[70]
NiO nanosheet	0.18	0.001–0.4	1138	[71]
NiSDCN/GCE	0.028	0.0001–10.20	1297	[1]
NiO@SDHCNSs/GCE	0.52	0.001–13	1697	This work

3.5. Reproducibility, stability and anti-interference property

In the present study, stability and reproducibility of the NiO@SDHCNSs hybrid nanocomposite modified glassy carbon electrode was examined by recording CV curves in the presence and absence of 1 mM glucose under 0.1 M NaOH electrolyte solution for 50 consecutive cycles at a scan rate of 50 mV s^{-1} (Fig. S7) and found that the glucose sensor retained ~98.6% of its initial oxidation peak current and without the presence of glucose, the redox couple of $Ni^{2+/3+}$ responsible for the catalytic activity of the electrode is showed sustained peak current and potential revealing an excellent stability and antifouling properties of the NiO@SDHCNSs/GCE for glucose sensor. In addition, the reproducibility of the glucose sensor was investigated by CV measurement at 1 mM glucose in 0.1 M NaOH at six newly prepared modified electrodes. All six electrodes exhibited similar current response and a relative stranded deviation (RSD) of 3.3%, indicating that the NiO@SDHCNSs/GCE modified electrode exhibits excellent reproducibility for glucose detection.

Furthermore, the selectivity of the NiO@SDHCNSs/GCE modified electrode for glucose was investigated in the interfering species such as dopamine (DA), uric acid (UA) and ascorbic acid (AA), these interfering species usually oxidize at the same potential on the unmodified electrodes in the non-enzymatic electrochemical sensor. Therefore, we have examined the capability of the synthesized activated S-doped carbon nanospheres based electrodes to distinguish the interference by measuring the amperometric responses by the addition DA, UA and AA 0.2 mM interference in 0.1 M NaOH containing 0.1 mM glucose at 0.55 V vs. SCE. Fig. 10 (I) shows the chronoamperometric responses of 0.1 mM glucose with other interferences, it is clear that the considerable electrocatalytic responses were obtained for glucose at the NiO@SDHCNSs/GCE, where there is no catalytic responses were observed for interfering species. The percentage of current increase towards glucose by the interference compounds is given as bar diagram Fig. 10 (II). These results suggest that the addition of DA, UA and AA are not shown significant increase of currents (<10%), indicating that the selectivity of the electrode is very good and it could be an outstanding candidate to detect the glucose in a practical sample. Selectivity of the fabricated electrode was also investigated with blood serum and urine samples, there was no appreciable current response for the interferences observed, whereas for glucose, significantly increased current noted. The reason behind the selectivity of the fabricated NiO@SDHCNSs/GCE sensor towards the glucose is the higher electron negativity of the glucose may diffuse closer to the electrode surface, more aggressively when compared with other interferences, hence, the electrode deserves good selectivity.

3.6. Real sample analysis

The control of diabetic related diseases is purely dependent upon the monitoring of glucose in blood serum and urine samples. Hence, the commercial applicability of the newly developed NiO@SDHCNSs modified GCE was further tested for the detection of glucose in human blood serum and urine samples by the standard addition method with the above experimental conditions with

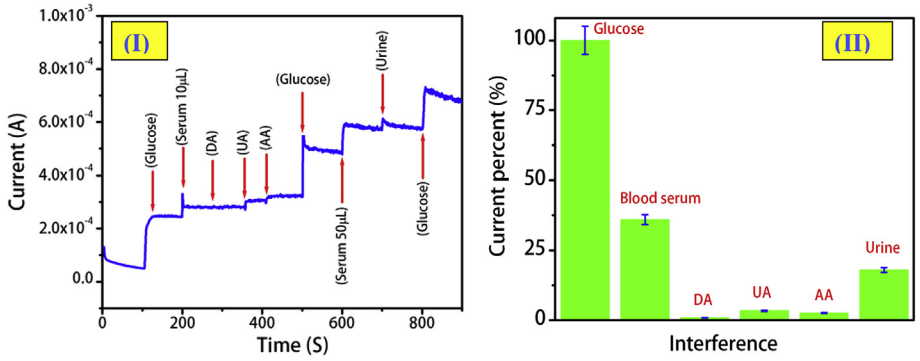

Fig. 10. (I) Chronoamperometric responses obtained for the 0.1 mM glucose oxidation at NiO@SDHCNSs with the consecutive addition of 0.2 mM AA, UA, DA and blood serum in 0.1 M NaOH, (II) The influence of interference compounds on the 0.1 mM glucose oxidation current (in %).

Table 2
Real sample analysis of glucose in human blood serum and urine samples using NiO@SDHCNSs/GCE modified electrode.

Samples	Content added (μM)	Content found (μM)	Recovery (%)
Blood serum	10	9.1	91
	30	29.5	98.3
	50	49.1	98.1
Urine sample	10	7.3	73
	30	27.2	90.6
	50	48.12	96.2

three replicate measurements of each sample. The known concentration of glucose was successively added into the blood and urine samples and its corresponding amperometric response of glucose was noticed. In both the cases, a good response is observed and the analytical results are listed in Table 2. The NiO@SDHCNSs glucose sensor is exhibited an excellent recovery in the range of 73%–98.3%, which guaranteed the potential applications of proposed sensor for practical non-enzymatic glucose sensor. The main advantages of the newly fabricated electrode for glucose sensor are; simple, cost effective eco-friendly hydrothermal preparation and simple drop casting electrode modification. Moreover, non-enzymatic sensor reported in this study requires only a tiny quantity of 10 μL (1 mg/mL) of NiO@SDHCNSs for electrode modification. The superiority of the present study can be attributed to the synergistic effect of the different components and unique hollow spheres like morphological structure with the high surface area and good electrical conductivity. Thus the facile synthesis strategy suggests that the NiO@SDHCNSs is a promising electrode material to construct the feasible non-enzymatic glucose sensor at a large scale.

4. Conclusions

In Summary, we have successfully synthesized NiO-SDHCNSs hybrid nanocomposites by using a simple hydrothermal method. A novel non-enzymatic biosensor was fabricated by using the NiO-SDHCNSs, exhibits favourable electrocatalytic properties for glucose oxidation in alkaline medium. Notably, compared to the bare NiO and SDHCNSs, the obtained NiO@SDHCNSs hybrid nanocomposite showed remarkably enhanced electrocatalytic activity towards glucose oxidation. The SDHCNSs could provide an excellent stable matrix supported to the Ni^{2+} ion adsorption by its S, O heteroatoms, where the electron clouds on the heteroatoms can interact with the 'd' orbital of Ni^{2+} ions to form $Ni(OH)_2$ and enwrap NiO nanoparticles with large effective surface area, which could act as electron transfer medium and promote the charge transfer between the electrode surface and glucose molecules by the unique hollow spheres like structures considered to be responsible for the effective glucose oxidation. Moreover, under the optimal conditions, this NiO@SDHCNSs/GCE constructed glucose biosensor shows more excellent performances such as high sensitivity (1697 $\mu A\ mM^{-1}\ cm^{-2}$), low detection limit (0.52 μM) and wide linear range (0.001–13 mM) and perfect selectivity to glucose in the presence of DA, UA, AA. Another advantageous feature of the NiO@SDHCNSs/GCE glucose sensor was applied in real biological samples (blood serum and urine) was gathered good response. All these results confirmed that NiO@SDHCNSS/GCE is a great promising electrode for practical glucose sensors applications.

Acknowledgement

The authors Dr. P. Shakkthivel would like to thank the DST-SERB, New Delhi, and (File No. EMR/2015/001475). Rajesh acknowledges University Grants Commission (UGC), New Delhi for Rajiv Gandhi National Fellowship (RGNF). We are acknowledging the USIC, Alagappa University, Karaikudi for XRD and Raman studies and STIC, Cochin University, Cochin for FESEM and TEM analysis.

Appendix A. Supplementary data

Supplementary data related to this article can be found at https://doi.org/10.1016/j.aca.2018.08.032.

References

[1] N. Karikalan, M. Velmurugan, S.M. Chen, C. Karuppiah, Modern approach to the synthesis of $Ni(OH)_2$ decorated sulfur doped carbon nanoparticles for the nonenzymatic glucose sensor, Appl. Mater. Interfaces 8 (2016) 22545–22553.
[2] R. Khan, R. Ahmad, P. Rai, L.W. Jang, J.H. Yun, Glucose-assisted synthesis of Cu_2O shuriken-like nanostructures and their application as nonenzymatic glucose biosensors, Sens. Actuators, B 203 (2014) 471–476.
[3] S. Radhakrishnan, S.J. Kim, Facile fabrication of NiS and a reduced graphene oxide hybrid film for nonenzymatic detection of glucose, RSC Adv. 5 (2015) 44346–44352.
[4] Li Wang, Y. Zhang, Y. Xie, J. Yu, H. Yang, L. Miao, Y. Song, Three-dimensional macroporous carbon/hierarchical Co_3O_4 nanoclusters for nonenzymatic electrochemical glucose sensor, Appl. Surf. Sci. 402 (2017) 47–52.
[5] J. Tian, S. Liu, Y. Luo, X. Sun, Fe(III)-based coordination polymer nanoparticles: peroxidase-like catalytic activity and their application to hydrogen peroxide and glucose detection, Catal. Sci. Technol. 2 (2012) 432–436.
[6] M.S. Steiner, A. Duerkop, O.S. Wolfbeis, Optical methods for sensing glucose, Chem. Soc. Rev. 40 (2011) 4805–4839.
[7] J. Luo, P. Luo, M. Xie, K. Du, B. Zhao, F. Pan, P. Fan, F. Zeng, Z. Zhang, G. Liang, A new type of glucose biosensor based on surface acoustic wave resonator using Mn-doped ZnO multilayer structure, Biosens. Bioelectron. 49 (2013) 512–518.
[8] N.J. Ronkainen, H.B. Halsall, W.R. Heineman, Electrochemical biosensors, Chem. Soc. Rev. 39 (2010) 1747–1763.
[9] Y. Huang, X. Dong, Y. Shi, C.M. Li, L.J. Li, P. Chen, Nanoelectronic biosensors based on CVD grown graphene, Nanoscale 2 (2010) 1485–1488.
[10] H. Hosseini, M. Behbahani, M. Mahyari, H. Kazerooni, A. Bagheri, A. Shaabani, Ordered carbohydrate-derived porous carbons immobilized gold nanoparticles as a new electrode material for electrocatalytical oxidation and determination of nicotinamide adenine dinucleotide, Biosens. Bioelectron. 59 (2014) 412–417.
[11] S. Kim, S.H. Lee, M. Cho, Y. Lee, Solvent-assisted morphology confinement of a nickel sulfide nanostructure and its application for non-enzymatic glucose sensor, Biosens. Bioelectron. 85 (2016) 587–595.
[12] D.M. Kim, J.M. Moon, W.C. Lee, J.H. Yoon, C.S. Chol, Y.B. Shim, A potentiometric non-enzymatic glucose sensor using a molecularly imprinted layer bonded on a conducting polymer, Biosens. Bioelectron. 91 (2017) 276–283.
[13] L. Wu, X. Zhang, H. Ju, Amperometric glucose sensor based on catalytic reduction of dissolved oxygen at soluble carbon nanofiber, Biosens. Bioelectron. 23 (2007) 479–484.
[14] X. Liu, L. Shi, W. Niu, H. Li, G. Xu, Amperometric glucose biosensor based on single-walled carbon nanohorns, Biosens. Bioelectron. 23 (2008) 1887–1890.
[15] C. Deng, J. Chen, X. Chen, C. Xiao, L. Nie, S. Yao, Direct electrochemistry of glucose oxidase and biosensing for glucose based on boron-doped carbon nanotubes modified electrode, Biosens. Bioelectron. 23 (2008) 1272–1277.
[16] S. Ci, T. Huang, Z. Wen, S. Cui, S. Mao, D.A. Steeber, J. Chen, Nickel oxide hollow microsphere for non-enzyme glucose detection, Biosens. Bioelectron. 54 (2014) 251–257.
[17] L.M. Lu, L. Zhang, F. Qu, H.X. Lu, X.B. Zhang, Z.S. Wu, S.Y. Huan, Q.A. Wang, G.L. Shen, R.Q. Yu, A nano-Ni based ultrasensitive nonenzymatic electrochemical sensor for glucose: enhancing sensitivity through a nanowire array strategy, Biosens. Bioelectron. 25 (2009) 218–223.
[18] P.V. Suneesh, K. Chandhini, T. Ramachandran, B.G. Nair, T.G.S. Babu, Tantalum oxide honeycomb architectures for the development of a non-enzymatic glucose sensor with wide detection range, Biosens. Bioelectron. 50 (2013) 472–477.
[19] Y. Mu, D. Jia, Y. He, Y. Miao, H.L. Wu, Nano nickel oxide modified non-enzymatic glucose sensors with enhanced sensitivity through an electrochemical process strategy at high potential, Biosens. Bioelectron. 26 (2011) 2948–2952.
[20] J. Huang, D. Wang, H. Hou, T. You, Electrospun palladium nanoparticle-loaded carbon nanofibers and their electrocatalytic activities towards hydrogen peroxide and NADH, Adv. Funct. Mater. 18 (2008) 441–448.
[21] P. Si, Y. Huang, T. Wang, J. Ma, Nanomaterials for electrochemical non-enzymatic glucose biosensors, RSC Adv. 3 (2013) 3487–3502.
[22] A. Safavi, N. Maleki, E. Farjami, Electrospun palladium nanoparticle-loaded carbon nanofibers and their electrocatalytic activities towards hydrogen peroxide and NADH, Biosens. Bioelectron. 24 (2009) 1655–1660.
[23] K.E. Toghill, L. Xiao, M.A. Phillips, R.G. Compton, The non-enzymatic determination of glucose using an electrolytically fabricated nickel microparticle

modified boron-doped diamond electrode or nickel foil electrode, Sensor. Actuator. B Chem. 147 (2010) 642–652.
[24] P. Luo, F. Zhang, R.P. Baldwin, Comparison of metallic electrodes for constant-potential amperometric detection of carbohydrates, amino acids and related compounds in flow systems, Anal. Chem. Acta 244 (1991) 169–178.
[25] A.M. Fermier, L.A.J. Colon, Capillary electrophoresis with constant potential amperometric detection using a nickel microelectrode for detection of carbohydrates, High- Resolut. Chromatogr. 19 (1996) 613–616.
[26] X. Niu, M. Lan, H. Zhao, C. Chen, Highly sensitive and selective nonenzymatic detection of glucose using three-dimensional porous nickel nanostructures, Anal. Chem. 85 (2013) 3561–3569.
[27] Y. Zhang, F.G. Xu, Y.J. Sun, Y. Shi, Z.W. Wen, Z. Li, Assembly of $Ni(OH)_2$ nanoplates on reduced graphene oxide: a two dimensional nanocomposite for enzyme-free glucose sensing, J. Mater. Chem. 21 (2011) 16949–16954.
[28] L.M. Lu, H.B. Li, F. Qu, X.B. Zhang, G.L. Shen, R.Q. Yu, In situ synthesis of palladium nanoparticle-graphene nanohybrids and their application in nonenzymatic glucose biosensors, Biosens. Bioelectron. 26 (2011) 3500–3504.
[29] T. Choi, S.H. Kim, C.W. Lee, H. Kim, S.K. Choi, S.H. Kim, E. Kim, J. Park, H. Kim, Synthesis of carbon nanotube–Nickel nanocomposites using atomic layer deposition for high-performance non-enzymatic glucose sensing, Biosens. Bioelectron. 63 (2015) 325–330.
[30] Y. Liu, H. Teng, H. Hou, T. You, Nonenzymatic glucose sensor based on renewable electrospun Ni nanoparticle-loaded carbon nanofiber paste electrode, Biosens. Bioelectron. 24 (2009) 3329–3334.
[31] Z.G. Zhu, L. Garcia-Gancedo, A.J. Flewitt, H.Q. Xie, E. Moussy, W.I.A. Milne, Critical review of glucose biosensors based on carbon nanomaterials: carbon nanotubes and graphene, Sensors 12 (2012) 5996–6022.
[32] P.A. Raymundo-pereira, A.M. Campos, F.C. Vicentini, B.C. Janegitz, C.D. Mendonca, L.N. Furini, N.V. Boas, M.L. Calegaro, C.J.L. Constantino, S.A.S. Machado, O.N. Oliveira Jr., Sensitive detection of estriol hormone in creek water using a sensor platform based on carbon black and silver nanoparticles, Talanta 174 (2017) 652–659.
[33] F.C. Vicentini, P.A. Raymundo-pereira, B.C. Janegitz, S.A.S. Machado, O. Fatibello-Filho, Nanostructured carbon black for simultaneous sensing in biological fluids, Sens. Actuators, B 227 (2016) 610–618.
[34] P.A. Raymundo-pereira, A.M. Campos, T.M. Prado, L.N. Furini, N.V. Boas, M.L. Calegaro, S.A.S. Machado, Synergy between Printex nano-carbons and silver nanoparticles for sensitive estimation of antioxidant activity, Anal. Chim. Acta 926 (2016) 88–98.
[35] P.A. Raymundo-pereira, A.M. Campos, C.D. Mendonca, M.L. Calegaro, S.A.S. Machado, O.N. Oliveira Jr., Printex 6L carbon nanoballs used in electrochemical sensors for simultaneous detection of emerging pollutants hydroquinone and paracetamol, Sens. Actuators, B 252 (2017) 165–174.
[36] A.M. Campos, P.A. Raymundo-pereira, C.D. Mendonca, M.L. Calegaro, S.A.S. Machado, O.N. Oliveira Jr., Size control of carbon spherical shells for sensitive detection of paracetamol in sweat, Saliva and Urine 2 (2018) 654–661.
[37] C. Han, S. Wang, J. Wang, M. Li, J. Deng, H. Li, Y. Wang, Controlled synthesis of sustainable N-doped hollow core-mesoporous shell carbonaceous nanospheres from biomass, Nano Res 12 (2014) 1809–1819.
[38] H. Du, Q. Wang, J. Yang, L. Guo, Y. Si, Y. Wang, H. Yuan, Facile carbonaceous microsphere templated synthesis of Co_3O_4 hollow spheres and their electrochemical performance in supercapacitors, Nano Res 6 (2013) 87–98.
[39] W. Wei, Z. Wang, Z. Liu, Y. Liu, L. He, D. Chen, A. Umar, L. Guo, J. Li, Metal oxide hollow nanostructures: fabrication and Li storage performance, J. Power Sources 238 (2013) 376–387.
[40] Y. Wang, X. Wang, M. Antonietti, Polymeric graphitic carbon nitride as a heterogeneous organocatalyst: from photochemistry to multipurpose catalysis to sustainable chemistry, Angew. Chem. Int. Ed. 51 (2012) 68–89.
[41] P.R. Solanki, M.K. Patel, A. Ali Md, B.D. Malhotra, A chitosan modified nickel oxide platform for biosensing applications, J. Mater. Chem. B 3 (2015) 6698–6708.
[42] R. Sathiyamoorthi, P. Santhosh, P. Shakkthivel, T. Vasudevan, LiNi0.8Co0.2–xTixO2 nanoparticles: synthesis, structure, and evaluation of electrochemical properties for lithium ion cell application, J. Solid State Electrochem. 11 (2007) 1665–1669.
[43] P. Yang, X. Tong, G. Wang, Z. Gao, X. Guo, Y. Qin, NiO/sic nanocomposite prepared by atomic layer deposition used as a novel electrocatalyst for nonenzymatic glucose sensing, ACS Appl. Mater. Interfaces 7 (2015) 4772–4777.
[44] F.T. Thema, E. Manikandan, A. Gurib- Fakin, M. Maaza, Single phase Bunsenite NiO nanoparticles green synthesis by Agathosma betulina natural extract, J. Alloy. Comp. 657 (2016) 655–661.
[45] K. Ghosh, M. Kumar, T. Marubyama, Y. Ando, Tailoring the field emission property of nitrogen-doped carbon nanotubes by controlling the graphitic/pyridinic substitution, Carbon 48 (2010) 191–200.
[46] P. Veerakumar, S.M. Chen, R. Madhu, V. Veeramani, C.T. Hung, S.B. Liu, Nickel nanoparticle-decorated porous carbons for highly active catalytic reduction of organic dyes and sensitive detection of Hg (II) ions, Appl. Mater. Interfaces 7 (2015) 24810–24821.
[47] C. Falco, N. Baccile, M.M. Titirici, Morphological and structural differences between glucose, cellulose and lingo cellulosic biomass derived hydrothermal carbons, Green Chem. 13 (2011) 3273–3281.
[48] A. Kruse, E. Dinjus, Hot compressed water as reaction medium and reactant: properties and synthesis reactions, J. Supercrit. Fluids 39 (2007) 362–380.
[49] J. Ryu, Y.W. Suh, D.J. Suh, D.J. Ahn, Hydrothermal preparation of carbon microspheres from mono-saccharides and phenolic compounds, Carbon 48 (2010) 1990–1998.
[50] S.A. Wohlgemuth, R.J. White, M. Willinger, M.M. Titirici, M.A. Antonietti, One-pot hydrothermal synthesis of sulfur and nitrogen doped carbon aerogels with enhanced electro catalytic activity in the oxygen reduction reaction, Green Chem. 14 (2012) 1515–1523.
[51] C. Billaud, S.B. Merimee, L. Louarme, J. Nicolas, Effect of glutathione and Maillard reaction products prepared from glucose or fructose with glutathione on polyphenoloxidase from apple—I: enzymatic browning and enzyme activity inhibition, Food Chem. 84 (2004) 223–233.
[52] S. Liu, J. Tian, L. Wang, Y. Zhang, X. Qin, Y. Luo, A.M. Asiri, A.O. Al- Youbi, X. Sun, Hydrothermal treatment of grass: a low-cost, green route to nitrogen-doped, carbon-rich, photoluminescent polymer nanodots as an effective fluorescent sensing platform for label-free detection of Cu(II) ions, Adv. Mater. 24 (2012) 2037–2041.
[53] D. Sun, R. Ban, P.H. Zhang, G.H. Wu, J.R. Zhang, J.J. Zhu, Hair fiber as a precursor for synthesizing of sulfur- and nitrogen-co-doped carbon dots with tunable luminescence properties, Carbon 64 (2013) 424–430.
[54] S.A. EI-Safty, Synthesis, characterization and catalytic activity of highly ordered hexagonal and cubic composite monoliths, J. Colloid Interface Sci. 319 (2008) 477–488.
[55] G.C. Zhao, L. Zhang, X.W. Wei, Z.S. Yang, Myoglobin on multi-walled carbon nanotubes modified electrode: direct electrochemistry and electrocatalysis, Electrochem. Commun. 5 (2003) 525–829.
[56] S. Vaidyanathan, J.Y. Cherng, A.C. Sun, C.Y. Chen, Bacteria-Templated NiO nanoparticles/microstructure for an enzymeless glucose sensor, Int. J. Mol. Sci. 17 (2016) 1–16.
[57] I. Danaee, M. Jafarian, F. Forouzandeh, F. Gobal, M.G. Mahjani, Impedance spectroscopy analysis of glucose electro-oxidation on Ni-modified glassy carbon electrode, Electrochim. Acta 53 (2008) 6602–6609.
[58] J. Wang, W. Bao, L. Zhang, A nonenzymatic glucose sensing platform based on Ni nanowire modified electrode, Anal. Methods 4 (2012) 4009–4013.
[59] T.G. Babu, T. Ramachandran, B. Nair, Single step modification of copper electrode for the highly sensitive and selective non-enzymatic determination of glucose, Microchimica Acta 169 (2010) 49–55.
[60] K.K. Naik, A. Gangan, B. Chakraborty, S.K. Nayak, C.S. Rout, Enhanced nonenzymatic glucose-sensing properties of electrodeposited $NiCo_2O_4$-Pd nanosheet: experimental and DFT investigations, ACS Appl. Mater. Interfaces 9 (2017) 23894–23903.
[61] G. Baskaya, Y. Yildiz, A. Savk, T.O. Okyay, S. Eris, H. Sert, F. Sen, Rapid, sensitive, and reusable detection of glucose by highly monodisperse nickel nanoparticles decorated functionalized multi-walled carbon nanotubes, Biosens. Bioelectron. 91 (2017) 728–733.
[62] B. Zhao, T. Wang, L. Jiang, K. Zhang, M.M.F. Yuen, J.B. Xu, X.Z. Fu, R. Sun, C.P. Wong, NiO mesoporous nanowalls grown on RGO coated nickel foam as high performance electrodes for supercapacitors and biosensors, Electrochim. Acta 192 (2016) 205–215.
[63] Z. Cui, R. Sun, Q. Nie, Controllable preparation of hierarchically core-shell structure NiO/C microspheres for non-enzymatic glucose sensor, J. Aalloys and Compounds 632 (2015) 402–407.
[64] J. Yang, M. Cho, C. Pang, Y. Lee, Highly sensitive non-enzymatic glucose sensor based on over-oxidized polypyrrole nanowires modified with $Ni(OH)_2$ nanoflakes, Sensor. Actuator. B Chem. 211 (2015) 93–101.
[65] L. Wang, Y. Tang, L. Wang, H. Zhu, X. Meng, Y. Chen, Y. Sun, X.J. Yang, P. Wan, Fast conversion of redo couple on $Ni(OH)_2$/C nanocomposite electrode for high-performance nonenzymatic glucose sensor, J. Solid State Electochem. 19 (2015) 851–860.
[66] B. Zhang, Y. He, B. Liu, D. Tang, Nickel-functionalized reduced graphene oxide with polyaniline for non-enzymatic glucose sensing, Microchim. Acta 182 (2015) 625–631.
[67] Z. Liu, Y. Guo, C. Dong, A high performance nonenzymatic electrochemical glucose sensor based on polyvinylpyrrolidone-graphene nanosheets-nickel nanoparticles-chitosan nanocomposites, Talanta 137 (2015) 87–93.
[68] P. Lu, J. Yu, Y. Lei, S. Lu, C. Wang, D. Liu, Q. Guo, Synthesis and characterization of nickel oxide hollow spheres-reduced graphene oxide-nafion composite and its biosensing for glucose, Sensor. Actuator. B Chem. 208 (2015) 90–98.
[69] Y. Shu, Y. Yan, J. Chen, Q. Xu, H. Pang, X. Hu, Ni and NiO nanoparticles decorated metal-organic framework nanosheets: facile synthesis and high-performance nonenzymatic glucose detection in human serum, ACS Appl. Mater. Interfaces 9 (2017) 22342–22349.
[70] Y. Ni, J. Xu, Q. Liang, S. Shao, Enzyme- free glucose sensor based on heteroatom-enriched activated carbon (HAC) decorated with hedgehog-like NiO nanostructure, Sensor. Actuator. B Chem. 250 (2017) 491–498.
[71] H. Zhang, S. Liu, Nanoparticles-assembled NiO nanosheets templated by graphene oxide film for highly sensitive non-enzymatic glucose sensing, Sensor. Actuator. B Chem. 238 (2017) 788–794.